since 1961

Baltica

BALTICA Volume 34 Number 1 June 2021: 27–46
https://doi.org/10.5200/baltica.2021.1.3

Topography of the Aleutian Trench south-east off Bowers Ridge, Bering Sea, in the context of the geological development of North Pacific Ocean

Polina Lemenkova

Lemenkova, P. 2021. Topography of the Aleutian Trench south-east off Bowers Ridge, Bering Sea, in the context of the geological development of North Pacific Ocean. *Baltica, 34 (1),* 27–46. Vilnius. ISSN 0067-3064.
Manuscript submitted 5 August 2020 / Accepted 3 April 2021 / Available online 20 June 2021

Abstract. The research is focused on the topographic modelling and mapping of the Aleutian Trench. The study area is situated in the Bering Sea, a marginal sea located northernmost of the Pacific Ocean, between Alaska and Kamchatka Peninsula. The geological setting of the region is characterized by the subduction of the oceanic Pacific Plate below the continental North American Plate. Other features include high seismic activity along the Aleutian island arcs bordering the oceanic seafloor. The objective of this paper is to explore the interaction between the geophysical setting affecting the relief of the seafloor by using geoinformation techniques and geological analysis. In the hypothesis of this study, variations in the geophysical fields as independent variables are reflected in the morphology of the seafloor, which can be observed using data visualization by the advanced cartographic scripting solutions. The open source high-resolution topographic map (ETOPO1), marine free-air gravity and Bouguer gravity anomaly data were used and integrated to investigate the potential correlation between the geophysical, geological, tectonic and topographic settings of the Bering Sea. Our main method includes bathymetric mapping of the area with publicly available bathymetric data using GMT. Materials include open source data: ETOPO1 raster grid with 1 arc-minute resolution, EGM96 gravity and vector contour layers of GMT. The research included complex thematic mapping of the region, including topographic, contour, geodetic and geophysical mapping, 3D modelling and geomorphological plotting of the 30 cross-section segments of the trench located SE off the Bowers Ridge. According to the processed ETOPO1 dataset, the minimal depth is -8480 m and the mean is -3089.154 m. The geoid undulations model shows that the majority of the gravity values lie in the interval between -10 and 20 m with the lowest values along the trench. The statistical histogram shows that the most common depth value in the segment of the Aleutian Trench is -4800 m, occurring 1722 times. The profile linear trend modelling was done with four different approaches of the regression model ($y = f(x) + e$) by weighted least squares (WLS) with arguments: 1) $m_2t = a + bt$ (polynomial model degree one); 2) $m_3t = a + bt + ct^2$ (polynomial model degree two); 3) $m_4t = a + bt + ct^2 + d\cos 2\pi*t + e\sin 2\pi*t$ (polynomial model with Fourier series one); and 4) additional plotting residuals. Surface modelling was performed using xyz modelling from the ASCII data enlarging fragment towards SE of the Bowers Ridge. The tested functionality of modules of GMT presented an effective cartographic scripting toolset enabling a precise topographic mapping and 3D modelling. The paper contributes to a more detailed understanding of the Pacific Ocean seafloor bathymetry, more specifically of the selected segment of the Aleutian Trench near Bowers Ridge area.

Keywords: *GMT; cartography; geology; 3D modelling; geophysics; gravity*

✉ *Polina Lemenkova (pauline.lemenkova@gmail.com) Schmidt Institute of Physics of the Earth, Russian Academy of Sciences, Bolshaya Gruzinskaya Str. 10, Bld. 1, Moscow, 123995, Russian Federation*

INTRODUCTION

Understanding the geomorphic form and shape of the deep-sea trenches is crucial for modelling their geophysical and geological phenomena, because different shapes affected by the lithosphere movements reveal details in the tectonic evolution of the region. Various factors affect the formation of deep-sea trenches, among which are tectonic plate movement, subduction dynamics of the underlying slab into the deep mantle seismic activities in the study area, e.g. submarine earthquakes (Shepard 1963), and geological phenomena identifying the characteristics of the submarine geomorphology of the trench based on geological data modelling and submarine geomorphology (Tibaldi, Bonali 2017; Lemenkova 2018a, 2018b; Yogodzinski *et al*. 2015; Münker *et al*. 2004).

The seafloor is constantly deforming under the impact of plate tectonic processes modelling the shape of the ocean floor. This activity is one of the fundamental issues of the marine geology. However, proper techniques to map the marine environment and bathymetry visualizing and modelling deep-sea regions are still developing (Wadge 1992; Schenke, Lemenkova 2008; Suetova *et al*. 2005; Lemenkova 2019a, 2019b; Wessel, Smith 1991). The study of the submarine landforms, such as oceanic trenches, has technical limitations due to the often remote and inaccessible location of the study object. Therefore, machine learning data modelling algorithms are an effective tool for marine mapping. This study uses Generic Mapping Tools (GMT), a cartographic toolset for mapping seafloor regions using shell scripts and developed methodology (Wessel, Smith 1991; Lemenkova 2019c, 2019d).

A particular challenge in the geospatial mapping of the seafloor are the dynamic processes that lead to the formation of the landforms. Submarine geological modelling should therefore encompass not only the landforms of the trench, but also its explicit links with tectonics, seismicity in the study area, earthquakes repeatability and magnitude, oceanological parameters (current direction and strength) and lithology (nature and properties of the underlying rocks).

With this study we address the question why the geophysical setting affects the relief of the seafloor and investigate interaction among free-air marine gravity, the dependence of topographic position along the trench on the varying geoid gravity values and the trend of the bathymetry profiles. The geoinformation techniques and geological analysis were used to solving the problem of geospatial analysis and coherency of the multi-source data used in this study.

Hence, the aim of this study is to explore the interaction between the geophysical setting affecting the relief of the seafloor by investigating the factors of regional geological evolution, tectonic history and variability in regional geophysical fields which greatly influenced the depth and landforms of the seafloor affecting the lithosphere in the southern region of the Bering Sea. The goal of the performed geomorphological mapping of the Bering Sea submarine regions is to visualize the seafloor landforms and features of the selected segment of the Aleutian Trench by using a multi-disciplinary approach of the scripting cartographic techniques and geological analysis.

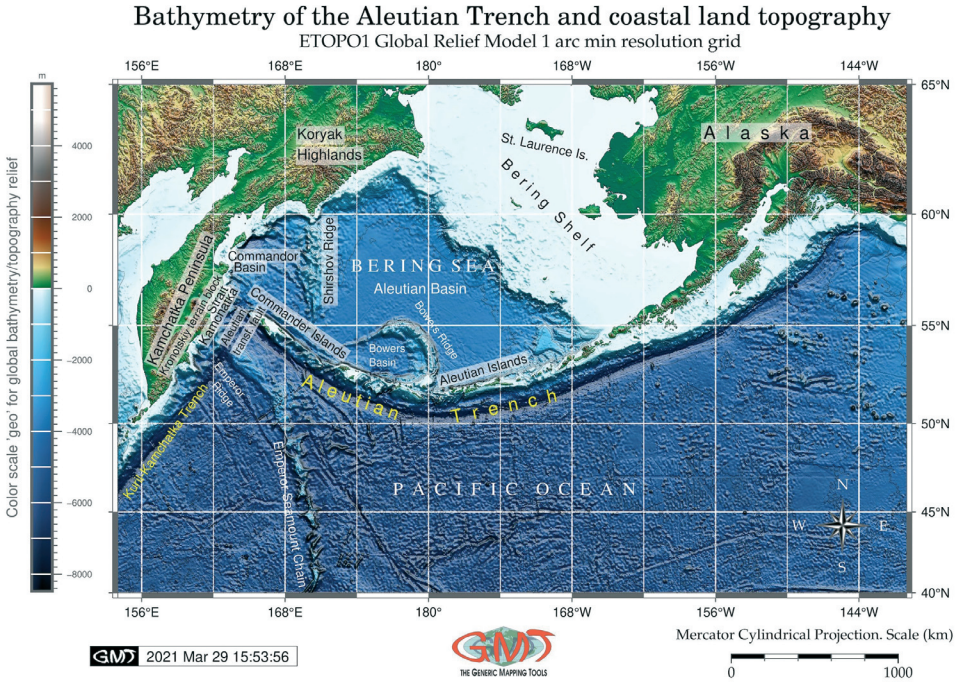

Fig. 1 Topographic map of the Bering Sea basin and the Aleutian Arc. Source: author

According to the hypothesis of this study, variations in the geophysical fields as independent variables are reflected in the morphology of the seafloor, which can be observed using data visualization by the advanced cartographic scripting solutions. Automated mapping by means of GMT makes geospatial analysis more effective today, since it enables to more focus on the geological data analysis rather than on technical aspects of the GIS-based mapping routine. Since the GMT is an open source toolset, the required material resources for cartographic processing only consist of the installed GMT and the collected data. Therefore, this study presents several code snippets to explain the efficient methods of GMT in more details.

The added value of this paper contributing to the existing studies on the Bering Sea consists in the novel approaches by cartographic scripting solving the needs to distinguish the geomorphology of the Aleutian Trench. Deep-sea trenches have a wide variety of geomorphological shapes that can be analysed through the cross-section techniques: slope steepness (smooth, steep, gentle slope), convex, asymmetric, V-formed, U-formed, and so on. Therefore, since not all deep-sea trenches are the same, it is important to model and map them to distinguish their unique geometry by using advanced cartographic solutions.

Rapid evolution of mapping approaches presents changed ways of mapping that makes the cartographic data processing more effective through faster workflow and more accurate maps based on the machine-based graphics. Modern map production often faces a strong time pressure and high requirements for map quality. This can be done by the application of GMT though its scripting paradigm, which consists in its logical and automated procedures of modular syntax.

Understanding the geomorphology of the oceanic trenches and surrounding seafloor is crucial in the comprehension of the Earth's tectonic evolution. Knowing the geomorphology of the deep-sea trenches assists in solving the problems of the correlation among factors affecting its formation, which can be formulated in the key questions: How do the tectonic plates movements shape the general morphology of the deep-sea trench? How do the seismicity and volcanism in the area of the trench increase the sedimentation intake and accumulation which may change the present form of the trench (e.g. sediment-starved or sediment-filled)? How does the particle size and load intensity contribute to the filling of the trench by sediments? Since the individual features of the gradient and the depth of the slopes of each trench vary, what are the major factors that shape the current form of the trench (caused by the tectonic movements and lithosphere processes in each particular region of the trench)? Finally, the ocean currents velocity also contributing to sedimentation may be a subject of additional studies with regard to the deep-sea trenches.

Since the middle of the 20th century along with rapid technological development of the bathymetric survey, the oceanic seafloor shape and morphology were largely used and discussed by scientific communities (Frohlich *et al*. 1982; Lundgren *et al*. 1995; Mortera-Gutiérrez *et al*. 2003; Vasquez *et al*. 2015; Beniest *et al*. 2016, 2018; Johnson *et al*. 2017; Beniest 2017; Dumke *et al*. 2018). Then, the progress in methods of data analysis and cartographic visualization introduced a new relationship between oceanic seafloor and tectonic history: seafloor spreading and formation of the submarine landforms (Fisher *et al*. 1987; Ely *et al*. 2016; Leat *et al*. 2016; Beniest *et al*. 2017; Schmid *et al*. 2020; Beniest, Schellart 2020; Lemenkova 2021a; Cloetingh *et al*. 2021).

Qualitative visualization of the spatial raster grids introduced the notion of conceptual neighbourhood (Freksa 1991), which refers to the geological, geophysical and topographic datasets aimed to identify correlations with the geomorphological landform of the trench corresponding to their spatial relationships (Pullar, Egenhofer 1988). Particularly, the relationship between geological setting, distribution of tectonic lineaments, properties of rocks (density, magmatism) underlying seafloor, oceanic geophysics and submarine geomorphology was not henceforward representable using a linear rapport because of their complex properties and nature. Accurate and systematic mapping of geomorphological features of the oceanic seafloor and deep-sea trenches based on high-resolution datasets (such as ETOPO1) provides a factual dataset for geomorphological interpretation and analysis of such correlation between topographic features, geophysical and geological setting.

A combined representation of the topographic and geophysical relationships with a comparison of the geomorphological modelling is a non-straightforward task from both cognitive geological and technical cartographic points of view. Some of these tasks are linked to the perceiving and representing geomorphological phenomena as 2D and 3D spatial models and overlaying gravimetric datasets with topographic maps. In this sense, a GMT-based visualization provides an appropriate description of the geographic relationships that apply in spatial dimensions by adjusting cartographic projections, grid dimensions, comparative and statistical analysis of the results.

The submarine geomorphological mapping exercise of this paper aims at visualizing and analysing landform features based on the combination of computer-based modelling and plotting through GMT and published literature of the geological setting of the study area located in the Bering Sea and Aleutian Trench. Variations in geomorphic local and regional features include variable seabed texture fabric: breaks

and smooth changes in the slope, conical and linear local depressions and/or submarine ridges. The GMT-based mapping of the geomorphological features of the Aleutian Trench in a selected digitized segment is undertaken at a consistent resolution (1 arc minute grid of ETOPO1) appropriate for the project which enabled to map in details of complex landforms. Larger scales were used for enlarged maps to better visualize the segment of the Bowers Ridge.

The Bering Sea, compared to other marginal seas of the Pacific Ocean is worth special attention due to its contrasting topography. The differences in bathymetry of the submarine margin of the continent are notable in western and eastern parts of the Bering Sea which depends on the age of the crystalline basement.

REGIONAL SETTING

Topographic location

The studies feature is the Aleutian Trench, an oceanic trench located in the Bering Sea, a marginal sea situated in the northernmost part of the Pacific Ocean (Udintsev *et al*. 1959; Murray 1945). The Aleutian Island Arc is placed on a submarine ridge separated from the Kamchatka Peninsula by the deep (> 4000 m) Kamchatka Strait. The topography of the Aleutian Island Arc is dissected by a long, narrow elevated feature that extends along the trench with relative heights between 400 and 1000 m, dividing the Aleutian Island Arc into several blocks. The geomorphology of the continental slope is characterized by a rather steep, stepped ledge with valleys and blocks. The seafloor of the southern Bering Sea reaches depths up to 3000 to 3300 m, where it smoothly transforms to the flat seafloor bottom of the Aleutian and Commandor basins with depths of 3700 to 4000 m, separated by a block of the Shirshov Ridge (depth of 3000 m).

Variations in the topography of the continental margin are contrasting in western and eastern parts of the Bering Sea, which depends on the age of the crystalline basement. The shelf of the Mesozoic platform of Chukotka, which connects to the shelf of the Mesozoic platform of Alaska, has a considerable width (up to 500–600 km) presenting a vast erosional plain formed in Beringia, then levelled by processes of abrasion and accumulation during flooding in the Pleistocene. The surface of the plain lies at depths of 80–120 m, and the outer edge of the shelf at depths of 120–180 m. The thickness of the sedimentary cover of the Bering Sea shelf is uneven: up to 3–4 km in the depressions of the Mesozoic platform basement, interrupted by several islands (St. Lawrence, St. Matthew, permafrost-covered volcanic island Nunivak, Pribilof Islands and the Diomede Islands). A different morphology of the continent's underwater margin is observed along Cenozoic of the Koryak Highlands and Kamchatka. Shelf abrasion terrace is narrow there, only 20–50 km, with depths up to 120–180 m. The continental slope is steep with many small submarine canyons. The sedimentary cover on the shelf and the slope is very thin, so that the foundation exposed in many places.

Geological setting

The Aleutian Island Arc is a huge mountain structure with a complex double structure separating the basin of the Bering Sea from the Pacific Ocean. Its mountain range stretches from the shores of North America to the shores of Eurasia in the form of a crescent arc with a radius of ca. 1500 km, with a centre near Cape Navarin. The ridge of the Aleutian Islands is mostly submarine and only appears above sea level by its peaks – by the Commander Islands and Aleutian ridges, Alaska and Kenai peninsulas. The total length of the Aleutian Island Arc reaches 3000 km.

The Aleutian Islands include rocks of many ages and types: hornfels, hornblende gneiss, slate, schist, granulite, granodiorite, varieties of granite (biotite and hornblende granite). The metamorphic rocks of Palaeozoic age in western Aleutians have undergone recrystallization. The presence of crystalline rocks of continental type proves that a large land mass must have existed in the vicinity in the Mesozoic or Palaeozoic times. The bedrock source of the boulders in western Aleutian Islands was not seen and may not be exposed. Therefore, the relative ages of the granitic and metamorphic rocks could not be definitely determined (Coats 1956). The granitic rocks might be younger however, because most of them lack directional textures, proving that they have not been metamorphosed.

The crystalline basement surface of the Mesozoic structures on the Alaskan Shelf of the Bering Sea forms an extensive marginal depression where the seafloor surface gradually sinks to the edge of the shelf, reaching depths of ca. 3000 m, gradually deepening further to the seafloor bottom of the basin (Kurnosov 1981). According to the magnetic anomalies, the basin of the Bering Sea formed during the Mesozoic and is a relic of the ancient Kula Plate according to the palaeotectonic reconstructions (Gorbatov *et al*. 2000).

The flat bottom of the Aleutian Trench seafloor is filled with sediments. According to the data of deep-water drilling (Udintsev 1987), the sediment stratum is represented by two layers. The lower layer has an age from Late Cretaceous to Late Miocene. It is composed of the hemipelagic sediments consisting of clay and silt-sized grains of terrigenous origin, biogenic material from the Aleutian Island Arc and marine or-

ganisms. This layer is consistently overlying the oceanic crystalline basement, gently inclined towards the foot of the Aleutian arc slope. The thickness of this layer is 200–400 m. The upper layer is represented by the horizontally accumulated turbidite deposits that unconformably overlie the hemipelagic sediments of the lower layer forming the wedges containing the deposits. The age of the sediments is from the Late Miocene to the present time, with thickness gradually increasing westwards from 1000 to 3000 m. The west end of the Aleutian Island Arc is separated from the continent by the Kamchatka Strait with depths over 4000 m (Udintsev 1987).

The basement surface of the Cainozoic structures of the Aleutian Island Arc and the coast of Kamchatka sinks along a steep ledge towards the seafloor bottom with depths ranging from 5000 to 7000 m (Udintsev *et al*. 1963). The depths of the crystalline basement surface in the Aleutian Trench are ca. 1000 m higher compared to the present topography (Udintsev 1972). The metamorphic granite layer is absent on the seafloor of the marginal Bering Sea, as proved both by geophysical data analysis and results of the deep-sea drilling (Artyushkov *et al*. 1984; Udintsev 1987). Instead, a basaltic, or other type of volcanic, layer is located below the sedimentary cover. The Conrad and Moho discontinuity extends beneath the island arc and submarine elevations (Torne *et al*. 2020).

The geological composition of the andesitic substrate in Aleutian Trench results from the melts of the subducted Pacific oceanic crust (Kay 1978). The most widespread rocks in the region of the Aleutian Islands include high alumina andesite, basalt and intrusions of gabbro and granodiorite. Clay minerals found in the rocks include smectite, illite, chlorite (Kim *et al*. 2015). The upper crust lithology is composed of the metamorphic rocks in the granulite (or amphibolite) facies of metamorphism and magmatic intrusions. The crust transitions from oceanic to continental arc in the Aleutian Islands region (Fliedner, Klemperer 2000; Holbroock *et al*. 1999). The Aleutian Island Arc separated the Mesozoic Aleutian Basin and the Paleogene arcs of the Shirshov Ridge located on the eastern border of the Commander Basin, and the Bowers Ridge from the ocean bed. A young Commander Basin of the Bering Sea began to form in the rear of the arising island arcs in response to rising of asthenospheric material and the extension of the crust.

The geological historical processes contributed to the environmental uniqueness of the Aleutian Islands area (Rathburn *et al*. 2009). The granite, metamorphic and sedimentary lithologies are derived from the Alaskan continental margin, while igneous clasts could be derived from volcanic sources surrounding the Bering Sea (Dadd, Foley 2016). The striped pattern of magnetic anomalies is stretching from the region of the Aleutian Island Arc and trending approximately east-west is found south of the Aleutian Trench (Hayes, Heirtzler 1968). The magnetic anomalies are located along the axial parts of anticlinal folds and are caused by the deep blocks of the basalt layer (as in bathymetry) and variations in the chemistry or magnetism of the rocks in the Aleutian Island region, as studied in various works (Bingham, Stone 1972; Watts, Talwani 1974; Cande 1976). The striped pattern of magnetic anomalies is also observed parallel to the Aleutian Island Arc at the seafloor bottom of the Bering Sea basin.

Tectonic evolution

The tectonic history of the Aleutian Island Arc is deeply connected with Kuril-Kamchatka Trench, because the Aleutian Island Arc collides with the Kuril-Kamchatka Arc in the area of the Cape Kamchatka peninsula (Freitag *et al*. 2001). The Aleutian transform fault separated the Kronotskiy terrain block from the Pacific Plate during the major event in the tectonic history of the Pacific region which was a plate reorganization that occurred ca. 50 Ma (Vaes *et al*. 2019; Seton *et al*. 2015; Müller *et al*. 2016). The Bering Sea is located in an area where the Pacific Plate subducts under the North American Plate. During the Early Cretaceous, subduction of the Pacific Plate below the North America Plate initiated. This subduction is still ongoing presenting an example of ocean-ocean convergent zones in the region where currently the Bering Sea is located. The large and old Pacific Plate moves in N–NW direction with respect to North America where it is subducted beneath the southern Alaska and the Aleutian Island Arc (Drewes *et al*. 1961). The Aleutian and Commander Islands are colliding with the Kamchatka Peninsula Cape. The collision was initiated after the changed direction of plate motion in the Middle Eocene (ca. 40 Ma), with the last collision episodes having started recently (Gaedicke *et al*. 2000). During the Mesozoic and Tertiary, the Kamchatka–Aleutian junction was affected by the subduction in Kronotskiy subduction zone and collision of the Kronotskiy arc against North-East Eurasia margin (Hanna *et al*. 2020), leading to the formation and developing of four structural assemblages of the Kronotskiy arc terrane, which are characterized by the precollisional deformations in the accretionary wedge, the fore-arc basin and volcanic belt, and syn-collisional deformation of the entire Kronotskiy terrane and deformations in the foreland basin (Alexeiev *et al*. 2006).

The Aleutian Island Arc is classified as an accreting margin (Jicha, Kay 2018) with most of the arc having a well-developed frontal prism that formed in the Plio-Pleistocene. The Central Aleutian volcanic

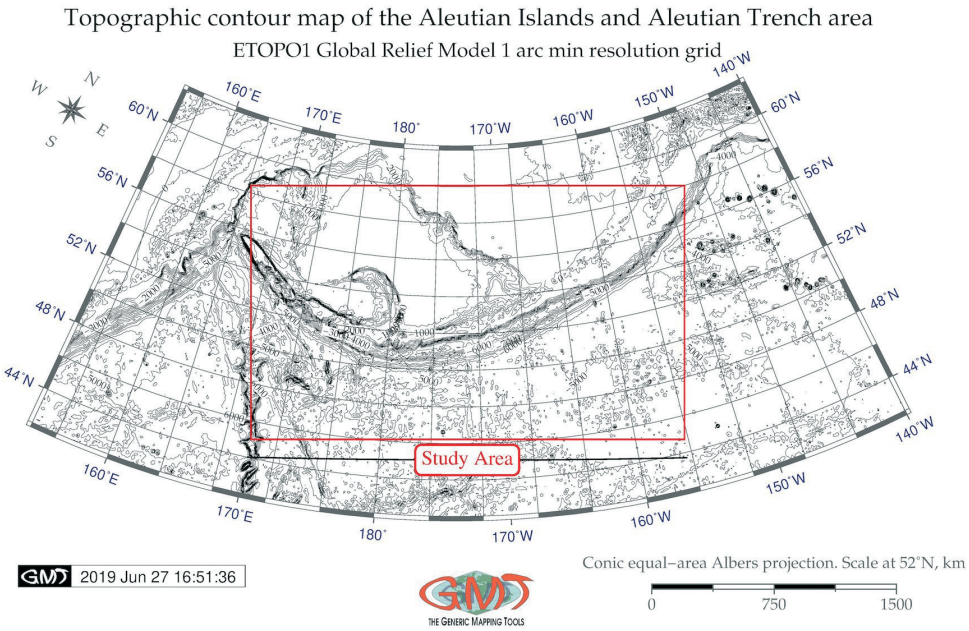

Fig. 2 Contour map of the study area. Source: author

front migrated 30–60 km northwards since the formation of the arc massif completed in the late Eocene. The Aleutian Trench has a weak coupling between the surface tectonic plate and subducting slabs (Yoshida 2017).

Seismicity and earthquakes

The Aleutian region is known for its seismic activity. In 1946, the seismicity of the Aleutian region caused a very severe tsunami (Bai *et al*. 2018), but other tsunamis originated in the Aleutian region affect far located regions (Ryan *et al*. 2014). Studies on the seismicity, earthquake sources and effects distribution in the region of the Aleutian Islands are presented in previous studies (Ekstrom, Engdahl 1989; Engdahl, Billington 1986). The seismic belt stretches along the NW and W margins of the Pacific Ocean and continues along the island arcs from the Aleutian Islands to New Zealand. In its central part, several seismically active zones are observed according to the direction of the island arcs in the western part of the Pacific Ocean. More detailed studies on the seismicity of the Aleutian Island Arc area are provided in relevant existing publications (Boyd *et al*. 1995; Liakopoulou-Morris *et al*. 1995; Estabrook *et al*. 1997; Gorbatov *et al*. 2001; López, Okal 2006).

There is a high seismic activity along the island arcs bordering the oceanic crust. Besides weak earthquakes, also some strong earthquakes with magnitudes of 7.0–8.5 and with hypocenters located under the island arcs with focal planes of 50–70° occurred (Litvin 1987). Using data from Harvard CMT catalogue since 1977, Mortera-Gutiérrez et al. (2003) reported three classes of focal mechanisms along the Aleutian Trench for the shallow, large earthquakes (<60 km depth with moment magnitudes Mw >4.5): (1) thrusting events of the interplate zone, (2) strike-slip fault events in the upper plate of the Aleutian Ridge, and (3) normal faulting events on the STS of the oceanic plate. That said, north of the Aleutian Trench most earthquakes point at thrust faulting. The depths of the earthquake hypocenters vary from 200–250 km to 600–700 km. Well-defined hypocenters reach depths of 200–300 km, with occasional hypocenters with greater depths (>500 km).

The thickness of the Earth's crust in the Bering Sea region varies and exceeds 30 km on the continental margin, is ca. 25 km thick under the Aleutian Island Arc, and only <10–12 km under the seafloor basin (Udintsev *et al*. 1980). The Earth's crust in the Commander depression is represented by almost a single velocity layer of 6.5 km/s. The Aleutian basin itself consists of two layers with velocities of 3.7–5.5 and 6.8–7.2 km/s, with Moho velocities of 8.0 km/s. The thickness of the Earth's crust in the Aleutian Trench is reduced to 8 km with velocities at 4.5–5.5 and 6.3–6.6 km/s (Litvin 1987).

MATERIALS AND METHODS

Data Listing

The precision in collecting, sorting and organizing data is the key for getting high-quality geospatial data, which will greatly influence the research output and final quality (Smith 1993; Wessel, Watts 1988). The data used in this research include vector

layers embedded in the GMT (coastlines) and high-resolution downloaded raster datasets: ETOPO1, xyz topographic and gravity datasets from the open public repositories of the USGS.

In this research, high-resolution geodata were collected from the United States Geological Survey (USGS) open source database geoid data EGM-96 (Lemoine *et al*. 1998), marine free-air gravity data (Sandwell, Smith 1997) and available embedded Geo-Information Systems (GIS) layers of the Generic Mapping Tools (GMT) (Wessel, Smith 1996; Smith, Sandwell 1997).

Mapping with GMT

This work is technically based on using the GMT, a cartographic scripting toolset, which has certain advantages over the existing traditional GIS, e.g. MapInfo, Erdas Imagine, QGIS, ArcGIS, widely used in the geosciences (Klaučo *et al*. 2013, 2014, 2017; Lemenkova *et al*. 2012). The scripting approach of the GMT is based on machine algorithms that can process data which results in printing quality and aesthetic values of the cartographical outputs. The layouts of the GMT are accurate with respect to the cartographic projection and scale.

GMT includes a formal programming foundation, i.e. a certain kind of scripting language with a set of minimal operators and flags required for the manipulation with cartographic commands, set-up regional projections and local adjustment (e.g. legends, grids, ticks, annotations). The main software used for this study is Generic Mapping Tools with various modules of which the functionality is described in the software documentation and release announcement (Wessel, Smith 1995; Wessel *et al*. 2013). GMT enables plotting of visual cartographic variables including (Bertin 1983) position, size, shape, value, colour, orientation, and texture of the cartographic elements.

The simplicity, clearness of graphic expression

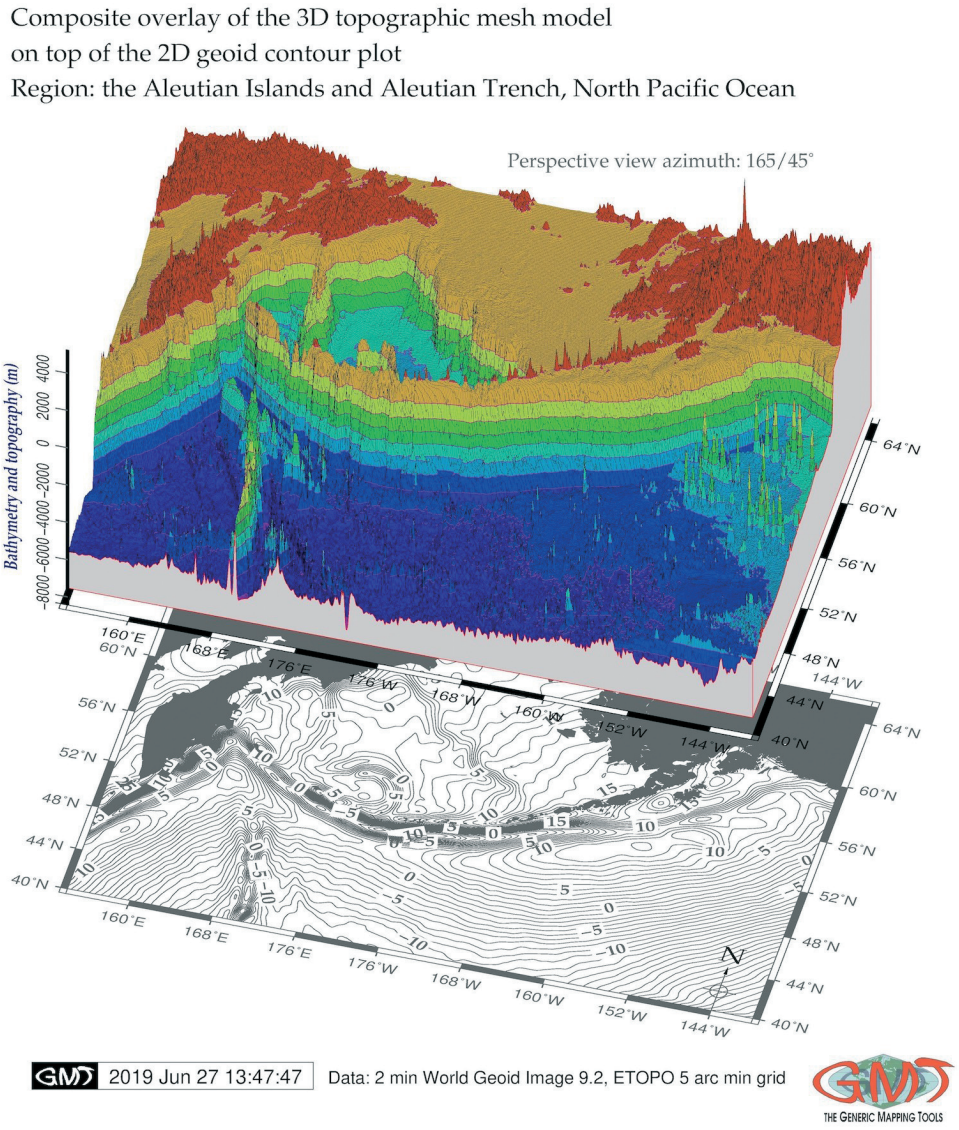

Fig. 3 Modelling 3D mesh grid of the Aleutian Islands and Aleutian Trench area. Source: author

and readability of maps is achieved through a detailed adjustment of the annotation fonts and cartographic elements. A wide variety of colour palettes (contrasting, neighbouring or complementary colours) supported by GMT enables to select the most suitable colours for representing continuous surfaces (gravity, geoid, topography) to balance graphic arts and technical methods for representing geographic phenomena (Imhof 1965). As a result, a special kind of aesthetics and beauty is inherent to a map plotted by GMT.

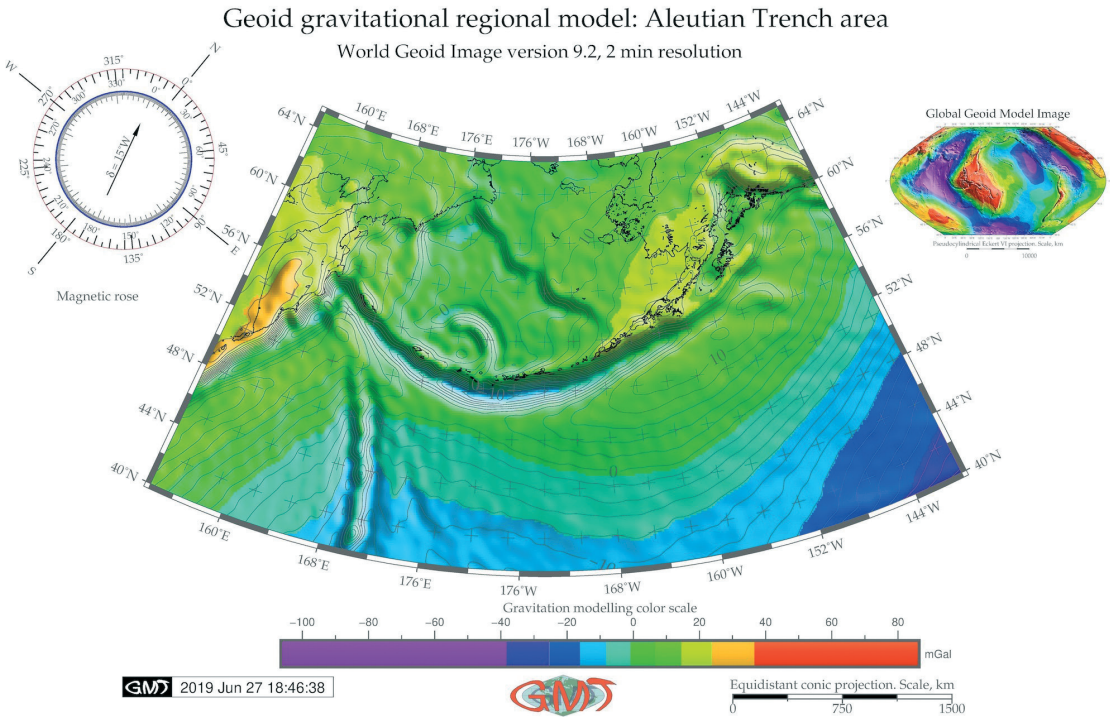

Fig. 4 Geoid model of the Bering Sea basin. Source: author

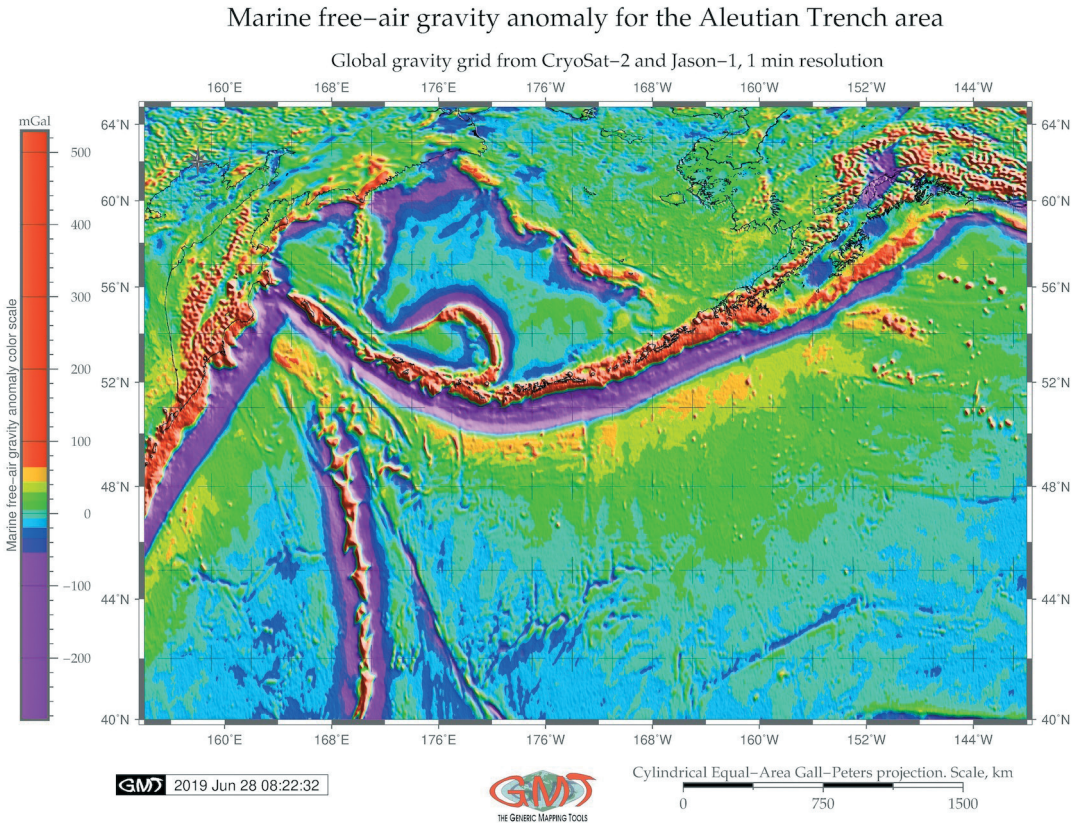

Fig. 5 Marine free-air gravity map of the Bering Sea basin. Source: author

The maps, using GMT, and the cartographic visualization presented in this paper are made according to the theoretical cartographic principles. These principles include the concept of semiotics and its three subdivisions (Freitag 1971): syntactics, that is, a syntax of a map; semantics, that is, producing a map with meaning and cartographic elements (Claramunt, Thériault 1996); and pragmatics, that is, the organization, general layout and contexts of the map layouts. Special GMT modules that are designed for plotting elements and base elements are 'pslegend' and 'psbasemap'. The general bathymetric map of this study is the ETOPO1 bathymetric 1 arc-minute resolution grid (Amante, Eakins 2009). The ETOPO1 global relief model was modelled with the 'grdimage' module of GMT (Fig. 1).

The initial grid was subset using the GMT module 'grdcut', which cuts off the region from the grid file within a window of 154°W – 220°W and 40°N – 65°N and saves it to the NetCDF format. The main drawing models used were: 'pscoast' module for mapping coastal lines and contours, 'psscale' module for mapping the colour legend, and 'pstext' module to add textual explanations on the map. The isolines were plotted with 1 m interval and annotations every 5 m using the GMT 'grdcontour' module.

The bathymetry was visualized using the 'geo' colour palette. The original data was derived from the sea-surface satellite altimetry measurements and ocean soundings provided by global geospatial sources (Amante, Eakins 2009). Therefore, the ETOPO1 includes existing bathymetry data and uses interpolated gravity values elsewhere. Based on an analysis of the ETOPO1 map (Fig. 1), the suitable segment was selected for plotting sample data on cross-section profiles and the series of the profiles was plotted for topographic analysis. Specifically, the segment was plotted as a line from start to end points (red thick points shown in Fig. 7) with the following coordinates: 180°W, 49.9°N to 172.0°W, 51.0°N.

Representing geological and geophysical data and the tectonic setting of the Barents Sea in one, referenced, map requires the understanding of their relationships within an integrated framework of the combined data in a GMT project. Combining several GMT modules allowed the computation and visualization of 2D and 3D models of the Aleutian Trench. The 3D map also includes a mesh model (Fig. 3), which shows that the study area rotated 165°/45° overlapping the contour map of the geoid. Several GMT modules were used following previous studies (Lemenkova 2020c), grdcut, grd2cpt, grdcontour, pscoast, grdview, logo, psconvert, in order to add cartographic elements on the map listed and summarized in Table 1.

The automated digitizing of the geomorphological profiles was done using the 'grdtrack' module of GMT. The simulation was programmed using GMT syntax using the ETOPO1 raster dataset as a base map.

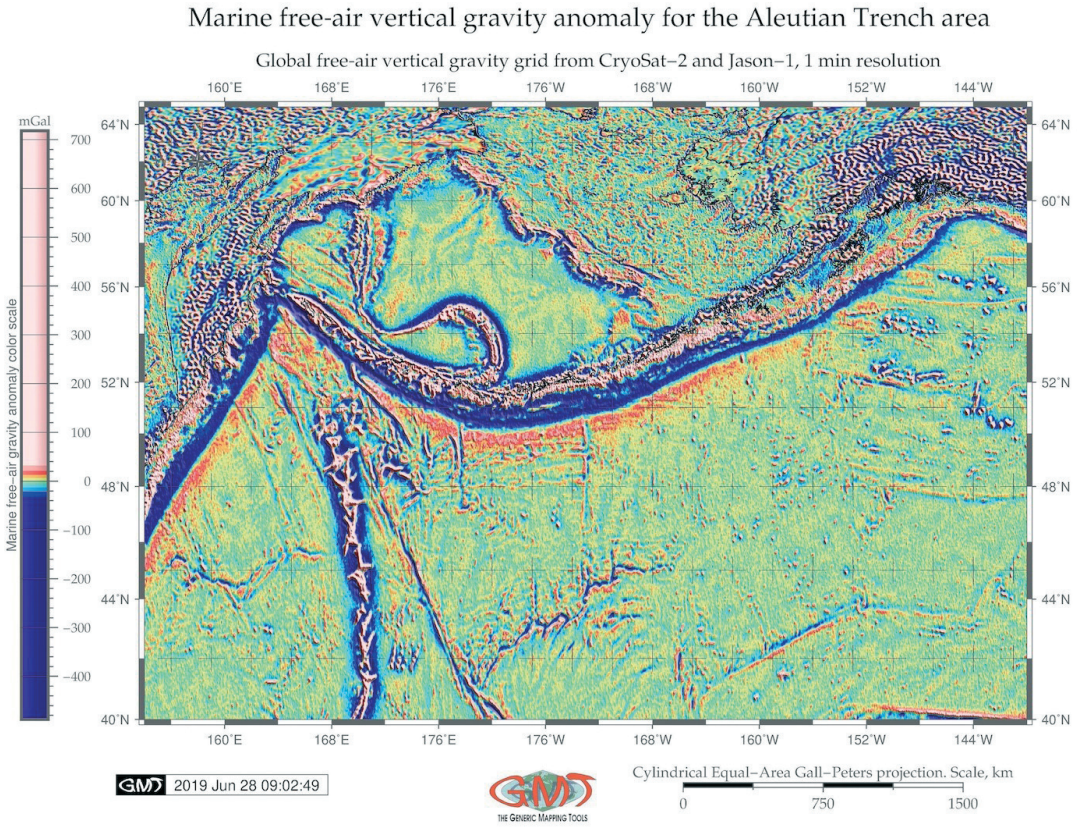

Fig. 6 Modelling free-air vertical marine gravimetry of the Bering Sea. Source: author

The model includes a systematic drawing of a cross-section consisting of 30 segments to evaluate the geomorphology of the Aleutian Trench. The cross-section (180.0°W 49.9°N (start point) 172.0°W 51.0°N (end point)) is 400 km long with 30 segments that are 2 km long and oriented perpendicular to the WSW-ENE oriented major cross-section (Fig. 7b). The segments are spaced 20 km apart (Fig. 7). From the start to end point of the major cross-section there is a set of points at which the perpendicular, 2-km wide segments were made. The distance between each two is 20 km. In total, there are 30 of the segments visualized in Fig. 7 as thin yellow lines parallel to each other with a 2 km distance between them. These segments were plotted automatically by GMT. The modelling consists of drawing a median line (red line on Fig. 7) and calculating error bars and an interval of the threshold (grey area) for the statistical dataset for all the segments (Fig. 7) using the GMT 'convert' module. The bathymetry was then mathematically modelled for line curvature (Fig. 8) and statistically processed (Fig. 9).

The coastlines, ticks and directional rose were added on the map using the GMT 'pscoast' module. The NetCDF grid format was processed as a grid file (Rew, Davis 1990). The cartographic routine includes adding the basic elements on the map, including ticks, gridlines, directional rose, legend and choosing a suitable projection. Further technical details are described in previous publications (Lemenkova 2019f, 2020b, 2021b). 3D modelling was done using the GMT 'grdview' module.

The CryoSat-2 and Jason-1 and gravity models are used to support geophysical investigations, geological prognosis as well as the geological resources management. The data included a raster grid developed by Lemoine *et al*. (1998) and tested methodology (Lemenkova 2020a). The GMT script used for modelling gravity includes the 'grdimage' and 'img2grd' modules. The combination of the GMT modules for modelling allows a proper visualization of the thematic maps.

To assist in the identification of the geomorphology of the Aleutian Trench, the bathymetric ETOPO1 data were contoured at 500 m intervals using the GMT module 'grdcontour' (Fig. 2). The geomorphic analysis process in GMT module 'trend1d' was applied to build statistical trends with four functional

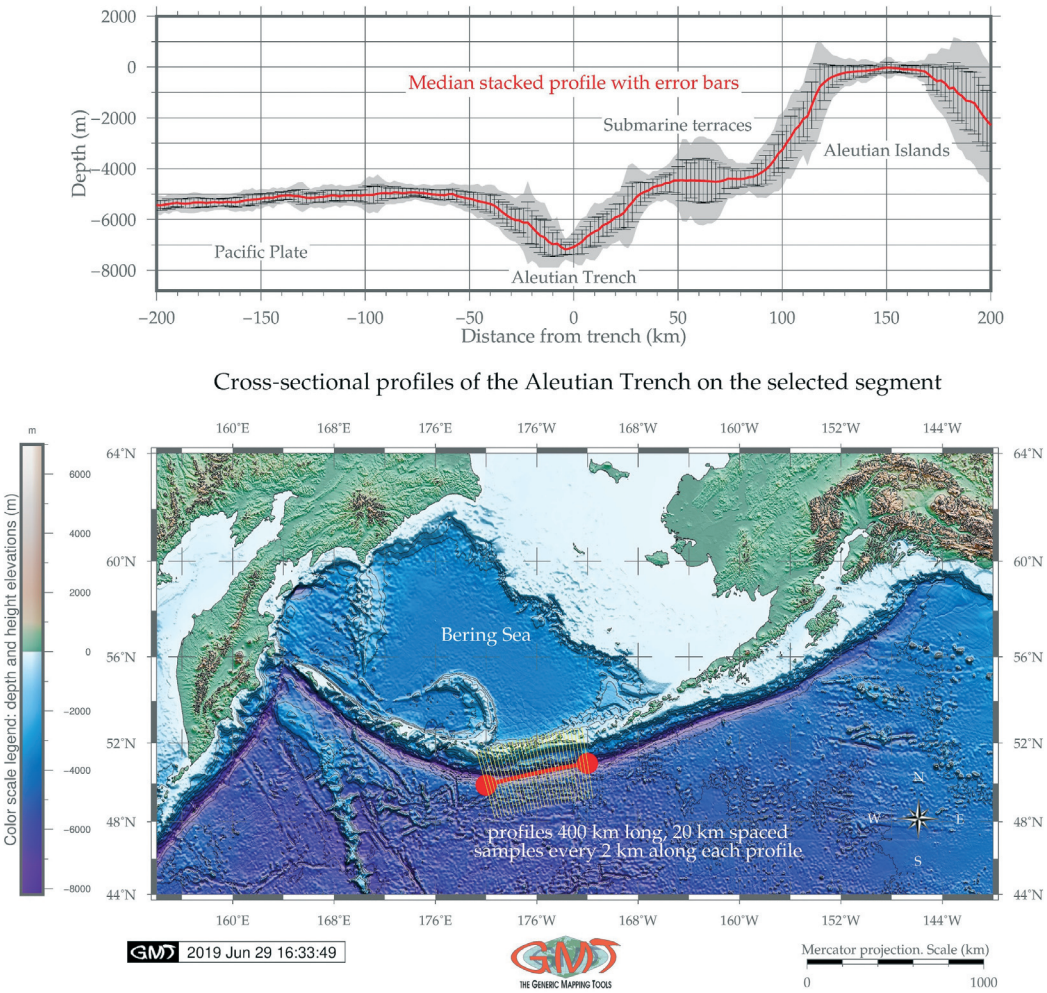

Fig. 7 Automatic digitizing of the cross-section profile in the study area. Source: author

approaches (Fig. 8) and visualization of the median and mean profiles (Fig. 7 and Fig. 8). The results of the surface modelling (Figs 10 and 11) were used by modelling an xyz dataset. The grid was smoothened prior to use by applying the 'blockmean' module of the GMT: it interpolated the original values in the table by a smoothing algorithm. The most important codes from the GMT scripts for modelling and mapping are presented and summarized in Table 1.

Statistical modelling with GMT

Statistical data modelling is an important tool for the analysis of data in geosciences (Lemenkova

Table 1 Summary of the GMT modules and examples of codes used for mapping

GMT module	Code snippet from the GMT script	Practical aim (purpose)
gmtset	gmt set FORMAT_GEO_MAP = dddF MAP_FRAME_PEN = dimgray \ MAP_FRAME_WIDTH = 0.1c \	Setting up general parameters of GMT (fonts, language, layout offset, style of coordinates, etc.)
img2grd	img2grd grav_27.1.img -R154/220/40/65 -GgravAT.grd -T1 -I1 -E-S0.1 -V	Conversion of the image which extracts a subset of the img file in Mercator projection
grd2cpt	gmt grd2cpt geoid.egm96.grd -Crainbow > geoid.cpt	Generating colour palette (here: example for geoid)
grdimage	gmt grdimage at_relief.nc -Catocean.cpt -R154/220/40/65 -JM6i -P –I + a15 + ne0.75 -Xc -K > $ps	Raster image visualization
pscoast	gmt pscoast -R -J -P -V -W0.25p -Df –B + t"Geoid gravitational regional model: Aleutian Trench area" -Bxg3f4a8 -Byg3f2a4 -O -K >> $ps	Plotting coast lines
grdcontour	gmt grdcontour geoid.egm96.grd -R -J -C2 -A5 -Wthinnest,dimgray -O -K >> $ps	Adding isolines
psbasemap	Add grid with major and minor lines gmt psbasemap -R -J -Bpxg12f6a12 -Bpyg5f5a5 -Bsxg6 -Bsyg5 –B + t"Bathymetry of the Aleutian Trench and coastal land topography" -O -K >> $ps	Adding base cartographic elements (grid, major and minor ticks, title and subtitle, scale, directional rose)
psscale	gmt psscale -R -J -CgravAT.cpt \ -Dg142/40+w11.0c/0.5c+v+o0.7/0i+m l \ -Bxg100f20a100+l"Marine free-air gravity anomaly colour scale" \ -I0.2 -By+lmGal -O -K >> $ps	Adding scale bar on the map
pstext	gmt pstext -R -J -N -O -K \ -F+jTL+f7p,5,black+jLB+a-270 -Gwhite@40 >> $ps << EOF 172.0 56.0 Shirshov Ridge EOF	Adding text on the map (left: example for annotating the Shirshov Ridge)
logo	gmt logo -Dx6.2/-2.2+o0.1i/0.1i+w2c -O -K >> $ps	Placing logo of GMT below the map
psrose	gmt psrose tableA2.txt -i1,4 -R0/1/0/360 \ -A7r -S1.0in \ -Glightsteelblue1 -Bx0.2g0.2 \ -By30g30+l"Bathymetric data distribution by cross-section profiles" \ -B + t"Aleutian Trench: Rose diagram on the cross-section profiles" + gghostwhite \ -M0.5c + e+gred2+n1c \ -W0.1p,red -Cm \ -UBL/-15p/-65p -Vv -K > $ps	Plotting rose diagram
pshistogram	gmt pshistogram table2.txt -i4 -R-8200/1000/0/20 -JX4.8i/2.4i -X3.6i \ -Bpxg1000a1000f100 + l"Bathymetry (m)" \ -Bpyg5a5f2.5 + l"Frequency distribution"+u" %" -Bsyg2.5 \ -BWSne + t"Aleutian Trench: Histograms of the depths values on the cross-section profiles"+gghostwhite -Gpowderblue \ -D+f6p,4 -L0.1p,dimgray -Z1 -W250 -N0+pred -N1+pblue -N2 + pgreen \ -O -K >> $ps	Plotting statistical histograms
pslegend	gmt pslegend -R -J -Dx1.0/-2.6+w5.0c+o-1.0/0.5c \ -F + pthick + ithinner + gwhite \ --FONT_ANNOT_PRIMARY = 8p -O -K << EOF >> $ps S 0.3c v 0.5c red 0.01c 0.6c Mean and standard deviation S 0.3c v 0.5c green 0.01c 0.6c LMS mode and scale S 0.3c v 0.5c blue 0.01c 0.6c Median and L1 scale EOF	Adding Legend
psconvert	gmt psconvert BathymetryAT.ps -A0.2c -E720 -Tj -Z	Converting the PostScript file to graphical format (e.g. JPG, TIFF). Example: to JPG with 720 dpi resolution, 0.2 cm margins
trend1d	gmt trend1d -Fxmr stackA2.txt -Np2,f1 + l1 > modelAT.txt	Modelling regression line
psxy	gmt psxy -R-200/200/-2000/1000 -J -Bpxag100f10 -Bsxg50 -Bpyaf+u"m" -Bsyg1000 -BWSne+gmintcream -W0.1 -Sc0.05c \ -Gred modelAT.txt -i0,2 -Y5.0c -O -K >> $ps	Plotting graph
echo	echo "m@-5@-(t) = a + b\267t + c\267t@+2@+ + d\267cos(2@~p@~t) + e\267sin(2@~p@~t)" | gmt pstext -R -J \ -F + f12p + cBL -Dj0.1i -Gcornsilk -O -K >> $ps	Adding annotations on the graph by Unix 'echo' utility and ASCII numeral system of Octal codes (the example is for texts in Fig. 8)
gdalinfo	gdalinfo at_relief.nc -stats	GDAL utility for inspecting the grid (min/max values)

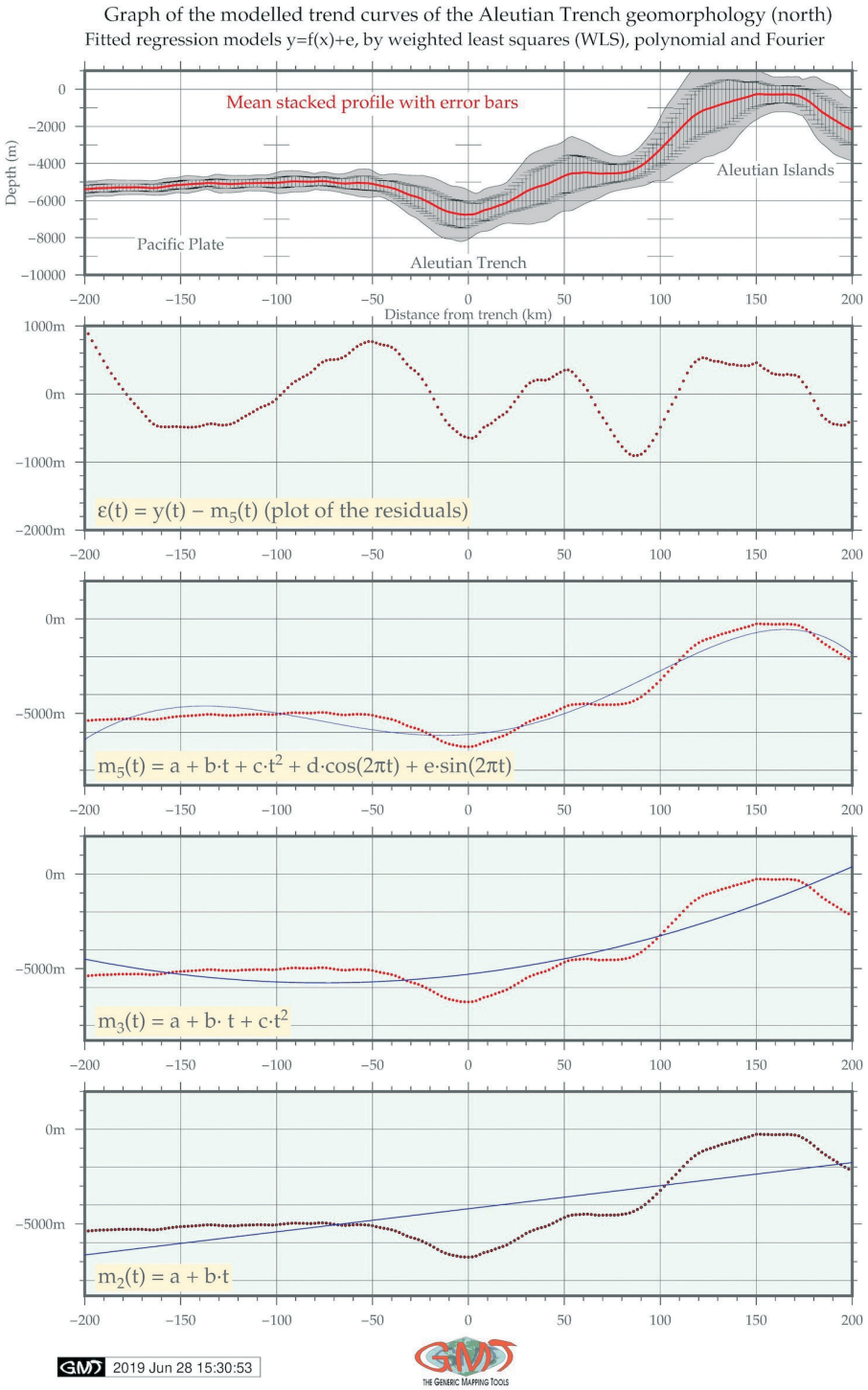

Fig. 8 Modelling trends for the relief of the mean cross-section profile. Source: author

2021c; Davis 2002; Lemenkov, Lemenkova 2021). Proper data interpretation should include testing several algorithms, selecting appropriate approaches and statistical packages (Jones *et al*. 2014). For this study, available techniques are used to model histograms (Lemenkova 2019e). The median derived the cross-section of the trench and shows the statistical visualization of the median stacked profiles with error bars (Fig. 7a).

RESULTS

The slopes of the Aleutian ridge have a complex stepped-block structure (Figs 7 and 8) with numerous ridges and canyons running parallel to the trench. The Aleutian Trench extends beyond the island arc on both sides, reaching the continental slopes of the Kamchatka Peninsula and Alaska. The seafloor of the trench is formed by a chain of the narrow depressions

with a rather flat seafloor bottom. The greatest depths are found in the centre of the trench (maximum depth is 8480 m). The depth of the processed ETOPO1 bathymetric data along the chosen profile ranges from -8480 m (bathymetry) to 5738 m (terrain areas).

The geoid gravitational model shows that the majority of the gravity values lie in the interval between -10 to 20 mGal with the lowest values along the trench. The most common depth value in the study area is 4800 m, occurring 1722 times. Four modelling approaches for the profile linear trend modelling were tested for the regression model (Fig. 8) ($y = f(x) + e$) by weighted least squares (WLS) with arguments: 1) $m_2t = a + bt$ (polynomial model degree one); 2) $m_3t = a + bt + ct^2$ (polynomial model degree two); 3) $m_4t = a + bt + ct^2 + d\cos 2\pi * t + e\sin 2\pi * t$ (polynomial model with Fourier series one); 4) additional plotting residuals. Finally, surface modelling was performed using xyz modelling from the ASCII data.

A clear correlation between the marine free-air gravity anomalies and the submarine topography can be seen in the Bering Sea. The free-air gravity anomaly of the Aleutian Basin and the Commander Basin have slightly positive free-air anomalies, the Shirshov Ridge and Bowers Ridge have moderately positive free-air anomalies, the Commander Islands and the Aleutian Islands have strong positive anomalies, and the Aleutian Trench is marked by strong negative anomalies (<- 100 mGal).

The Bouguer anomaly increases with a decreasing thickness of the Earth's crust from the continental margin to the seafloor of the Bering Sea basin. However, contrasting with the background of the intense positive anomalies of the seafloor of the Bering Sea basin, the submarine ridges Shirshov Ridge and Bowers Ridge are characterized by low Bouguer gravity anomaly values. This indicates a relative increase in the thickness of the Earth's crust below both ridges. Sharp gradients of marine free-air gravity anomalies are observed in the zone of the Aleutian Island Arc and the Aleutian Trench. There, the trench is characterized by a rather moderate positive free-air gravity anomaly which is much smaller than the anomaly of the oceanic seafloor.

The topographic modelling shows a highly detailed distribution of the bathymetric data along the segments of the cross-section (Fig. 9). The topographic analysis shows that the shelf of the Bering Sea is very wide in the NE and narrows towards NW. This controls the asymmetry in the bathymetry of the ocean floor. The surface of the shelf is mostly horizontal, with minimal bathymetric variation; however, in some areas there are locally some small valleys and elevations observed. The prevailing depths of the bathymetric features are about 60 to 90 m, reaching 120 to 140 m depth at the outer edge.

The statistical inventory of the bathymetric data is summarized in a histogram (Fig. 9) and shows that depths with ranges between 5600 and 5400 m occur 1106 times (8%); depths with ranges between 5400 and 5200 m occur 846 times (7%); and depths with ranges between 4900 and 5200 m occur 1297 times (11%). The highest values of 4900 and 4700 m occur 1722 times (13.2%). Significantly low values demonstrated shallow areas with depth ranges between 4500 and 3000 m with occurrence of below 200 (all

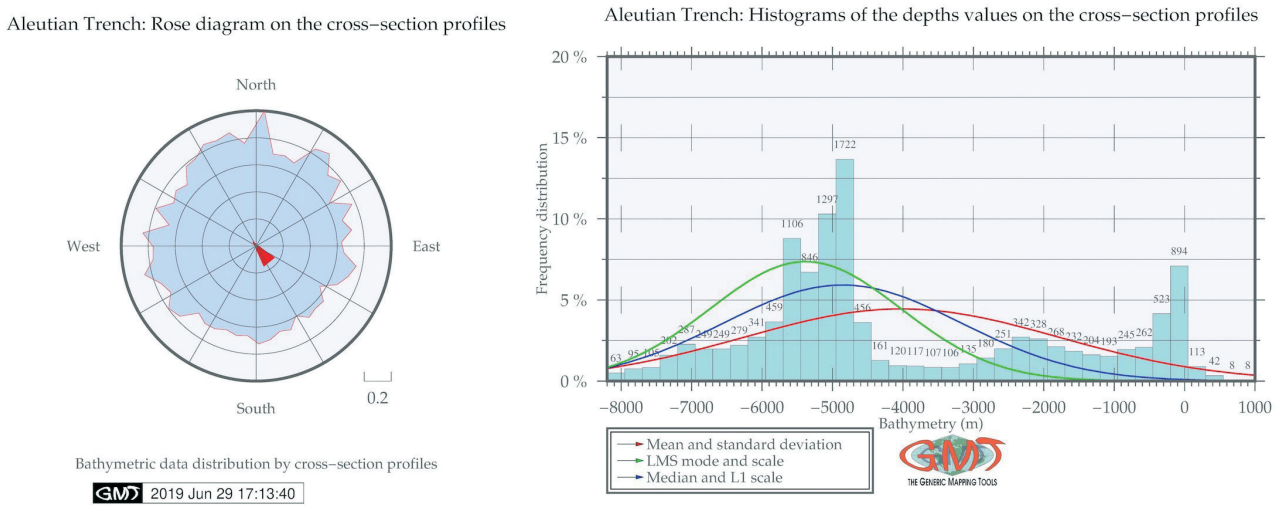

Fig. 9 Histogram chart showing the bathymetric data distribution (depths) by the profiles. The statistical inventory shows that depths with ranges between 5600 and 5400 m occur 1106 times (8%); depths with ranges between 5400 and 5200 m occur 846 times (7%); depths with ranges between 4900 and 5200 m occur 1297 times (11%). The highest values of 4900 and 4700 m are with 1722 occurrences (13.2%). Much lower values demonstrated shallow areas with depth ranges between 4500 and 3000 m with occurrence below 200 (all of them less than 2.5%). Values with ranges shallower than 500 m belong to the shelf areas near the Aleutian Islands adjusting the trench. Source: author

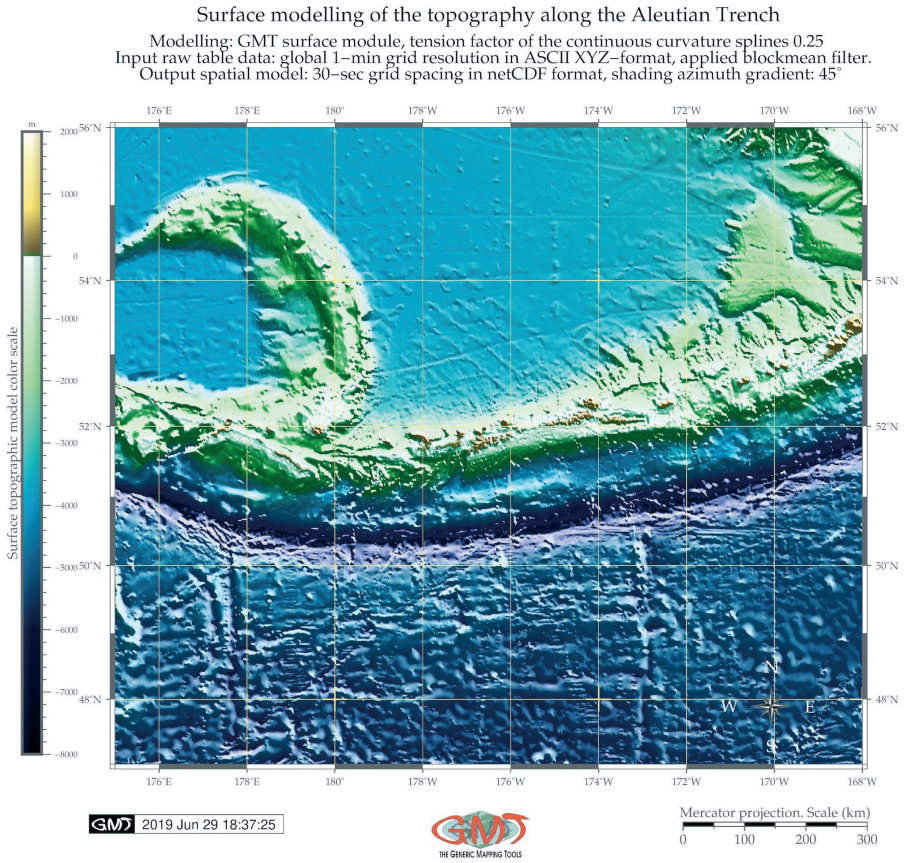

Fig. 10 Topographic surface modelling of the Bowers Ridge from the ASCII xyz data. Source: author

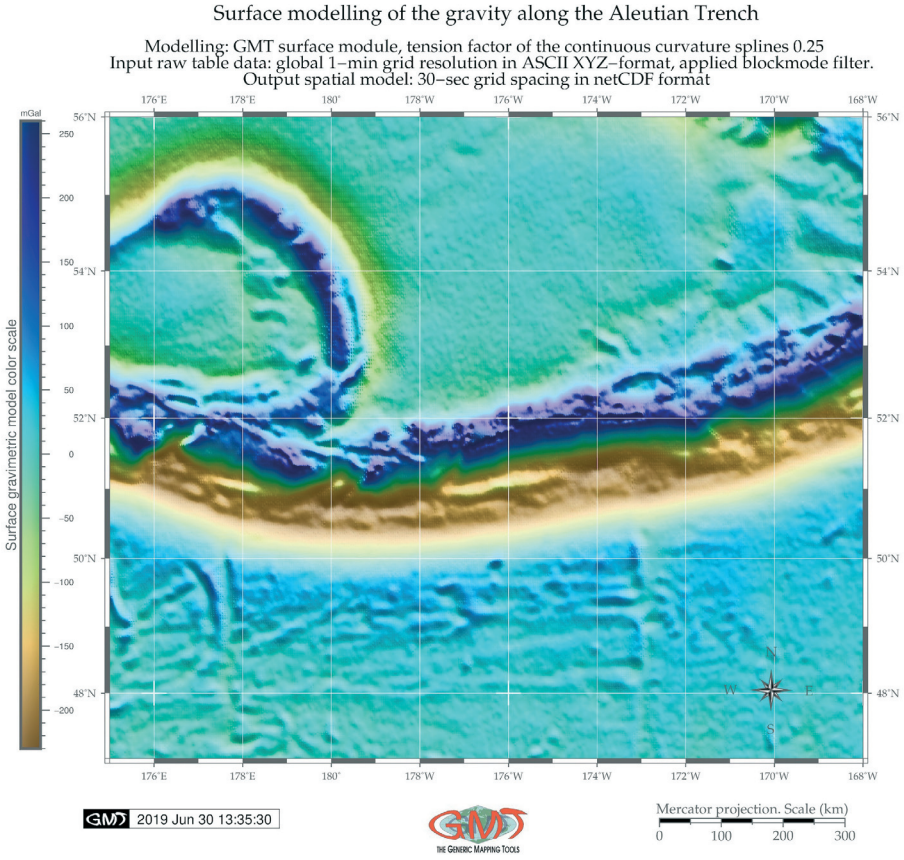

Fig. 11 Surface modelling of the gravity over Bowers Ridge from the ASCII xyz data. Source: author

of them less than 2.5%). Values with ranges shallower than 500 m belong to the coastal shelf areas near the Aleutian Islands adjusting the trench. A geomorphic analysis (Figs 8 and 3) shows that the NW of the trench, on the side of the island arc, has a steeper and shorter slope, with a series of marine terraces.

DISCUSSION

The geophysical mapping of the Bering Sea and geomorphological modelling of the selected segment of the Aleutian Trench was demonstrated using the GMT cartographic scripting toolset. The newly presented maps of the Aleutian Trench region support the hypothesis on the impacts of geophysical and tectonic evolution affecting the modern structure of the seafloor, which are indicated as differences in topographic shapes and variability of depth along the Aleutian Trench. The complexity of the geomorphic landforms and the response of topography to the impacts from geophysical processes and geological evolution presenting interactions between these factors in the basin of the Bering Sea is a challenging task to evaluate in a simplified way. The variability of the topography of the Bering Sea is notable on the presented maps. The basin of the Bering Sea is contrasting with its shelf (NE region) and outlined by the 3000 m isoline. It has the notable submarine uplifts: Shirshov Ridge, Bowers Ridge and Aleutian Island Arc which separate it to the western, eastern and southern parts, respectively: the Aleutian Basin, the Commander Basin and the Bowers Basin (Fig. 1).

The seafloor of these basins is presented by the accumulative abyssal plain. The maximum depths are 3887 m in the Aleutian Basin, 3828 m in the Commander Basin, and 3500 m in the Bowers Basin. The geomorphology of the Shirshov and Bowers Ridges has a fault block structure with asymmetric steep slopes and destructed surface levelled by the abrasion processes in the geological past. The bathymetry of the both ridges varies from 500 to 1000 m, with minimum depths of 559 m for the Shirshov Ridge and 256 m for the Bowers Ridge.

A subsequent analysis of the Bering Sea region seafloor in the context of geophysical and topographic setting showed that an effective cartographic model of the submarine topographic landforms depends on a range of factors presenting the interaction between the geophysical, geological and tectonic factors shaping the trench form. Besides, important are technical characteristics of the models themselves defined using GMT parameters, the geographic context in which models are placed (since western and eastern parts of the Pacific Ocean present trenches of various depths and shapes), and the interactions between data and cartographic approaches used for data processing (data formats, data resolution, data origin).

Visualizing submarine geomorphology provided the context and guidance for further geological and oceanographic discussions regarding hadal trench shape, occurrence of terraces, steepness of the slopes, location of canyons, as well as their distribution. The major results of the profile are the maximum depth of the trench of 8480 m, the asymmetric continental shelf, which is wider in the E and NE and much narrower in the W and SW. The geoid modelling shows that the majority of the geoid values lie in the interval between 10 to 20 mGal with the lowest values along the trench that proves the deficit of the landmasses in the depression of the trench. The analysis of the marine free-air gravity shows the data range from the minimum at -284.919 mGal to the maximum at 529.791 mGal with the mean at 5.037 mGal.

The major negative values of gravity lie exactly along the trench areas (including both Aleutian and Kuril-Kamchatka trenches visible on the map in Fig. 5), as well as along the Emperor Seamounts Chain and the Bowers Ridge and north of the Commander Basin (all values are coloured deep purple in Fig. 5). This seems to indicate regional coherency of the geophysical anomaly fields with bathymetry and topographic distribution of the negative and positive landforms in the basin of the Bering Sea. On the contrary, higher values of gravity (bright red colours in Fig. 5) clearly correspond to the distribution of the topographic landmasses in the Aleutian Trench.

The main result of our analysis is that bathymetry is distributed unequally along the study area in the trench, according to major distributions of the landforms and with respect to the location of the Aleutian Island Arc and Aleutian Trench having the crescent-arc geometric form in the south of the Bering Sea. The selected cross-section demonstrates that repeatability of depths variation between 5600 and 5400 m is 8%; repeatability of depth between 5400 and 5200 m is in approximately the same frequency of 7%; repeatability of depth between 4900 and 5200 m is 11%; and the highest values of 4900 and 4700 m occur in 13.2%, which are the most often values. Much lower values demonstrated shallow areas with depth ranges between 4500 and 3000 m with occurrence less than 2.5%. The values with ranges shallower than 500 m belong to the shelf areas near the Aleutian Islands adjusting the trench.

These results show that the geomorphology, geological setting and geophysical data are connected, because the model of the trench topographic shape represents a complex non-linear system depending on the approximated functionality of the variety of factors, such as geophysical, tectonic and geologic as the major driving forces sculpturing submarine bathymetry, with considerable uncertainty in the conditions of impact factors.

CONCLUSIONS

The geomorphology of the seafloor is driven by complex interactions among prevailing tectonic and geological settings as the most important factors contributing to the actual shape of the seabed. Some regional patterns in this correlation regarding the Aleutian Trench were noted, such as, for instance, a strong role of landmass distribution in gravity anomalies: negative and positive values in gravity grids mirroring the isolines of the depressions and islands in the seafloor topography, respectively.

Besides, the geological setting and tectonic evolution of the region are largely influenced by the geophysical process of tectonic plate subduction in which the Pacific Plate subducts under the North American Plate, forming a convergent boundary with the trench-arc system (Aleutian Trench and Aleutian Island Arc). The complexity of these tectonic processes consequently involved a series of faults and had a pronounced influence on the seafloor bathymetry across the Bering Sea, enabling to analyze their consequences for the topographic variability of the seafloor.

The paper discussed both methodological algorithms of the mapping and analysis of the geological evolution and characteristics of the study area based on the previous works. Traditionally, bathymetric mapping includes data of the sub-bottom echo sounder or swath bathymetric surveying (Kuhn *et al*. 2006; Gauger *et al*. 2007); however, this work demonstrated the use of the scripting approaches of the GMT used for the processing of the open source data on topography and geophysics of the Bering Sea region. Future work can consider the results of this paper illustrating the relationship between the geomorphology of the trench and the geological and geophysical setting.

The results of this study included the compiled bathymetry, gravity and geoid data obtained from the open access sources of geoinformation and applied the global grids for the region of the Bering Sea and Aleutian Trench in the North Pacific Ocean. The results of mapping and geomorphological cross-section modelling of the Aleutian Trench, as well as those derived from general statistical calculation of histograms (based on the 30 topographic segments of the cross-section of the Aleutian Trench) demonstrate a substantial variation of submarine topography of the seafloor reflecting geophysical conditions reflected in the varying values of marine free-air gravity anomalies (Faye's), vertical gravity anomalies, and the gravitational model of geoid.

The produced maps show high-resolution geometric features and shapes (observed using the map based on the 15-arc second resolution GEBCO grid). Several presented models and maps describe the geological, geophysical and geomorphic modelling of the study area, including an outline of the shell scripting, the model, and visualized maps. Advantages of the GMT demonstrated in the presented paper consist in its high efficiency for the cartographic workflow.

Geomorphological modelling through cross-sectioning and thematic geophysical mapping and geology and geomorphology interpretation revealed complex features such as fracture zones, ridges, abyssal plain and hills, seamounts and guyots on the seabed of the Bering Sea and in the Aleutian Trench. Visualizing submarine geomorphology provided the context and guidance for further geological and oceanographic discussions regarding hadal trench shape, occurrence of terraces, steepness of the slopes, location of canyons, as well as their distribution.

ACKNOWLEDGEMENTS

I am deeply grateful to Dr. Anouk Beniest (Assistant Professor from Vrije Universiteit Amsterdam, Netherlands) for careful reading, thoughtful review and numerous constructive comments regarding geology and tectonics. Her suggestions on methodology and critical remarks about the structure of the manuscript significantly improved the initial version of this manuscript and some of the maps. I also highly appreciate the review and feedback of one anonymous reviewer. This research has been implemented in the framework of the Project No. 0144-2019-0011, Schmidt Institute of Physics of the Earth, Russian Academy of Sciences.

REFERENCES

Alexeiev, D.V., Gaedicke, C. Tsukanov, N.V., Freitag, R. 2006. Collision of the Kronotskiy arc at the NE Eurasia margin and structural evolution of the Kamchatka-Aleutian junction. *International Journal of Earth Sciences (Geologische Rundschau) 95 (6)*, 977–993. https://doi.org/10.1007/s00531-006-0080-z

Amante, C., Eakins, B.W. 2009. *ETOPO1 1 Arc-Minute Global Relief Model: Procedures, Data Sources and Analysis*. NOAA Technical Memorandum, 19.

Artyushkov, E.V., Shlezinger, A.E., Yanshin, A.L. 1984. Tektonicheskiye struktury dna Mirovogo okeana [Tectonic structures of the World Ocean floor]. *Doklady AN SSSR* [*Reports of the USSR Academy of Sciences*] *275*, 148–150. [In Russian].

Bai, Y., Yamazakia, Y., Cheung, K.F. 2018. Amplification of drawdown and runup over Hawaii's insular shelves by tsunami N-waves from mega Aleutian earthquakes. *Ocean Modelling 124*, 61–74. https://doi.org/10.1016/j.ocemod.2018.02.006

Beniest, A. 2017. *From continental rifting to conjugate margins: insights from analogue and numerical modelling*. PhD Thesis. University Pierre et Marie Curie, Paris, France, 212 pp.

Beniest, A., Schellart, W.P. 2020. A geological map of the Scotia Sea area constrained by bathymetry, geological

data, geophysical data and seismic tomography models from the deep mantle. *Earth-Science Reviews 210*, 103391. https://doi.org/10.1016/j.earscirev.2020.103391

Beniest, A., Brun, J.P., Gorini, C., Crombez, V., Deschamps, R., Hamon, Y., Smit, J. 2016. Interaction between trench retreat and Anatolian escape as recorded by neogene basins in the northern Aegean Sea. *Marine and Petroleum Geology 77*, 30–42. https://doi.org/10.1016/j.marpetgeo.2016.05.011

Beniest, A., Koptev, A., Burov, E. 2017. Numerical models for continental break-up: Implications for the South Atlantic. *Earth and Planetary Science Letters 461*, 176–189. https://doi.org/10.1016/j.epsl.2016.12.034

Beniest, A., Willingshofer, E., Sokoutis, D., Sassi, W. 2018. Extending Continental Lithosphere With Lateral Strength Variations: Effects on Deformation Localization and Margin Geometries. *Frontiers in Earth Science 6*, 148. https://doi.org/10.3389/feart.2018.00148

Bertin J. 1983. *Semiology of graphics: diagrams, networks, maps*. University of Wisconsin Press.

Bingham, D.K., Stone, D.B. 1972. Palaeosecular Variation of the Geomagnetic Field in the Aleutian Islands, Alaska. *Geophysical Journal International 28 (4),* 317–335. https://doi.org/10.1111/j.1365-246X.1972.tb06796.x

Boyd, T.M., Engdahl, E.R., Spence, W. 1995. Seismic cycles along the Aleutian arc: Analysis of seismicity from 1957 through 1991. *Journal of Geophysical Research 100 (B1)*, 621–644. https://doi.org/10.1029/94JB02641

Cande, S.C. 1976. A Palaeomagnetic Pole from Late Cretaceous Marine Magnetic Anomalies in the Pacific. *Geophysical Journal International 44 (3),* 547–566. https://doi.org/10.1111/j.1365- 246X.1976.tb00292.x

Claramunt, C., Thériault, M. 1996. *Toward semantics for modelling spatio-temporal processes within GIS*. In: Kraak, M.J., Molenaar, M. (eds.), *Advances in GIS Research I*. London: Taylor & Francis, 27–43.

Cloetingh, S., Koptev, A., Kovács, I., Gerya, T., Beniest, A., Willingshofer, E., Ehlers, T.A., Andrić Tomašević, N., Botsyun, S., Eizenhöfer, P.R., François, T., Beekman, F. 2021. Plume-induced sinking of intracontinental lithospheric mantle: An overlooked mechanism of subduction initiation? *Geochemistry, Geophysics, Geosystems 22*, e2020GC009482. https://doi.org/10.1029/2020GC009482

Coats, R.R. 1956. Reconnaissance geology of some western Aleutian Islands, Alaska. *U.S. Geological Survey Bulletin 1028–E*, 83–100.

Dadd, K., Foley, K. 2016. A shape and compositional analysis of ice-rafted debris in cores from IODP Expedition 323 in the Bering Sea. *Deep Sea Research Part II: Topical Studies in Oceanography 125–126*, 191–201. https://doi.org/ 10.1016/j.dsr2.2016.02.007

Davis, J.C. 2002. *Statistics and Data Analysis in Geology*. 3-rd edition. Wiley.

Drewes, H., Fraser, G.D., Snyder, G.L., Barnett, H.F.J. 1961. Geology of Unalaska Island and adjacent insular shelf, Aleutian Islands, Alaska. *U.S. Geological Survey Bulletin 1028-S,* 583–676.

Dumke, S., Nornes, M., Purser, A, Marcon, Y., Ludvigsen, M., Ellefmo, S.L., Johnsen, G., Søreide, F. 2018. First hyperspectral imaging survey of the deep seafloor: High-resolution mapping of manganese nodules. *Remote Sensing of Environment 209*, 19–30. https://doi.org/10.1016/j.rse.2018.02.024

Ekstrom, G., Engdahl, E.R. 1989. Earthquake source parameters and stress distribution in the Adak Island region of the central Aleutian Islands, Alaska. *Journal of Geophysical Research 84*, 15499–15519. https://doi.org/10.1029/JB094iB11p15499

Ely, J.C., Gribble, E.A., Clark, C.D. 2016. The glacial geomorphology of the western cordilleran ice sheet and Ahklun ice cap, Southern Alaska. *Journal of Maps 12* (*1*), 415–424. https://doi.org/10.1080/17445647.2016.1234981

Engdahl, E.R., Billington, S. 1986. Focal depth determination of central Aleutian earthquakes. *Bulletin of the Seismological Society of America 76*, 77–93.

Estabrook, C.H., Weber, M., Kind, R. 1997. Generation of the teleseismic P-wave coda from Aleutian earthquakes. *Geophysical Journal International 130 (2),* 349–364. https://doi.org/10.1111/j.1365-246X.1997.tb05652.x

Fisher, M.A., von Huene, R., Smith, G.L. 1987. Reflections from midcrustal rocks within the Mesozoic Subduction Complex near the Eastern Aleutian Trench. *Journal of Geophysical Research 92 (B8),* 7907–7915. https://doi.org/10.1029/JB092iB08p07907

Fliedner, M., Klemperer S.L. 2000. Crustal structure transition from oceanic arc to continental arc, eastern Aleutian Islands and Alaska Peninsula. *Earth and Planetary Science Letters 179*, 567–579. https://doi.org/ 10.1016/S0012-821X(00)00142-4

Freitag, U. 1971. Semiotik und Kartographie. *KartographischeNachrichten 21*, 171–182.

Freitag, R., Gaedicke, C., Baranov, B., Tsukanov, N. 2001. Collisional processes at the junction of the Aleutian-Kamchatka arcs: new evidence from fission track analysis and field observation. *Terra Nova 13*, 433–442. https://doi.org/10.1046/j.1365-3121.2001.00375.x

Freksa, C. 1991. Conceptual neighbourhood and its role in temporal and spatial reasoning. *Technical Report FK1–146–91*, University of Munich, Institute of Information.

Frohlich, C., Billington, S., Engdahl, E.R., Malahoff, A. 1982. Detection and location of earthquakes in the Central Aleutian Subduction Zone using island and ocean bottom seismograph stations. *Journal of Geophysical Research 87* (*B8*), 6853–6864. https://doi.org/ 10.1029/JB087iB08p06853

Gaedicke, C., Baranov, B., Seliverstov, N., Alexeiev, D., Tsukanov, N., Freitag, R. 2000. Structure of an active arc-continent collision area: the Aleutian–Kamchatka junction. *Tectonophysics 325*, 63–85. https://doi.org/10.1016/S0040-1951(00)00131-1

Gauger, S., Kuhn, G., Gohl, K., Feigl, T., Lemenkova, P., Hillenbrand, C. 2007. Swath-bathymetric mapping. *Reports on Polar and Marine Research* 557, 38–45. https://doi.org/10.6084/m9.figshare.7439231

Gorbatov, A., Widiyantoro, S., Fukao, Y., Gordeev, E. 2000. Signature of remnant slabs in the North Pacific from P-wave tomography. *Geophysical Journal International 142 (1)*, 27–36. https://doi.org/10.1046/j.1365-246x.2000.00122.x

Gorbatov, A., Fukao, Y., Widiyantoro, S., Gordeev, E. 2001. Seismic evidence for a mantle plume oceanwards of the Kamchatka–Aleutian trench junction. *Geophysical Journal International 146 (2),* 282–288. https://doi.org/10.1046/j.0956-540x.2001.01439.x

Hanna, H.D., Liu, X.-M., Park, Y. R., Kay, S.M. Rudnick, R.L. 2020. Lithium isotopes may trace subducting slab signatures in Aleutian arc lavas and intrusions. *Geochimica et Cosmochimica Acta 278 (1)*, 322–339. https://doi.org/10.1016/j.gca.2019.07.049

Hayes, D.E., Heirtzler, J.R. 1968. Magnetic anomalies and their relation to the Aleutian Island Arc. *Journal of Geophysical Research 73 (14)*, 4637–4646. https://doi.org/10.1029/JB073i014p04637

Holbroock, W.S., Lizarraide, D., McGeary, S., Bangs, N., Diebold, J. 1999. Structure and composition of the Aleutian island arc and implications for continental crustal growth. *Geology 27(1)*, 31–34. https://doi.org/10.1130/0091-7613(1999)027<0031:SACOTA>2.3.CO;2

Imhof, E. 1965. *Kartographische Geländedarstellung*. De Gruyter, Berlin.

Jicha, B.R., Kay, S.M. 2018. Quantifying arc migration and the role of forearc subduction erosion in the central Aleutians. *Journal of Volcanology and Geothermal Research 360*, 84–99. https://doi.org/10.1016/j.jvolgeores.2018.06.016

Johnson, S.Y., Cochrane, G.R., Golden, N.E., Dartnell, P., Hartwell, S.R., Cochran, S.A., Watt, J.T. 2017. The California Seafloor and Coastal Mapping Program – Providing science and geospatial data for California's State Waters. *Ocean & Coastal Management 140*, 88–104. https://doi.org/10.1016/j.ocecoaman.2017.02.004

Jones, E., Oliphant, T., Peterson P. 2014. *SciPy: open source scientific tools for Python*. Available at http://www.scipy.org

Kay, R.W. 1978. Aleutian magnesianan desites: melts from subducted Pacific Ocean crust. *Journal of Volcanology and Geothermal Research 4,* 117–132.

Kim, S., Khim, B.-K., Cho, H.G. 2015. Clay mineral stratigraphy during the last 2.4 Ma at IODP Exp. 323 Site U1343 in the Bering Sea. *Marine Geology 359 (1)*, 163–168. https://doi.org/10.1016/j.margeo.2014.10.004

Klaučo, M., Gregorová, B., Stankov, U., Marković, V., Lemenkova, P. 2013. Determination of ecological significance based on geostatistical assessment: a case study from the Slovak Natura 2000 protected area. *Open Geosciences 5 (1),* 28–42. https://doi.org/10.2478/s13533-012-0120-0

Klaučo, M., Gregorová, B., Stankov, U., Marković, V., Lemenkova, P. 2014. Landscape metrics as indicator for ecological significance: assessment of Sitno Natura 2000 sites, Slovakia. *Ecology and Environmental Protection. Proceedings of the International Conference*. March 19–20, 2014. Minsk, Belarus, 85–90. https://doi.org/ 10.6084/m9.figshare.7434200

Klaučo, M., Gregorová, B., Stankov, U., Marković, V., Lemenkova, P. 2017. Land planning as a support for sustainable development based on tourism: A case study of Slovak Rural Region. *Environmental Engineering and Management Journal 2 (16)*, 449–458. https://doi.org/10.30638/eemj.2017.045

Kuhn, G., Hass, C., Kober, M., Petitat, M., Feigl, T., Hillenbrand, C.D., Kruger, S., Forwick, M., Gauger, S., Lemenkova, P. 2006. The response of quaternary climatic cycles in the South-East Pacific: development of the opal belt and dynamics behavior of the West Antarctic ice sheet. In: Gohl, K. (ed). *Expeditions programm Nr. 75 ANT XXIII/4, AWI.* https://doi.org/10.13140/RG.2.2.11468.87687

Kurnosov, V.B. 1981. *Geological history of the Bering Sea*. Vladivostok. DVNTS AN SSSR, 116 pp.

Leat, P., Fretwell, P., Tate, A., Larter, R., Martin, T., Smellie, J., Jokat, W., Bohrmann, G. 2016. Bathymetry and geological setting of the South Sandwich Islands volcanic arc. *Antarctic Science 28*, 293–303. https://doi.org/10.1017/S0954102016000043

Lemenkov, V., Lemenkova, P. 2021. Using TeXMarkup Language for 3D and 2D Geological Plotting. *Foundations of Computing and Decision Sciences 46 (3)*, 43–69. https://doi.org/10.2478/fcds-2021-0004

Lemenkova, P. 2018a. Factor Analysis by R Programming to Assess Variability Among Environmental Determinants of the Mariana Trench. *Turkish Journal of Maritime and Marine Sciences 4 (2)*, 146–155. https://arxiv.org/abs/1812.00989

Lemenkova, P. 2018b. R scripting libraries for comparative analysis of the correlation methods to identify factors affecting Mariana Trench formation. *Journal of Marine Technology and Environment 2*, 35–42. https://arxiv.org/abs/1812.01099

Lemenkova, P. 2019a. Statistical Analysis of the Mariana Trench Geomorphology Using R Programming Language. *Geodesy and Cartography 45 (2)*, 57–84. https://doi.org/10.3846/gac.2019.3785

Lemenkova, P. 2019b. AWK and GNU Octave Programming Languages Integrated with Generic Mapping Tools for Geomorphological Analysis. *GeoScience Engineering 65 (4)*, 1–22. https://doi.org/10.35180/gse-2019-0020

Lemenkova, P. 2019c. Topographic surface modelling using raster grid datasets by GMT: example of the Kuril-Kamchatka Trench, Pacific Ocean. *Reports on Geodesy and Geoinformatics 108*, 9–22. https://doi.org/10.2478/rgg-2019-0008

Lemenkova, P. 2019d. GMT Based Comparative Analysis and Geomorphological Mapping of the Kermadec and Tonga Trenches, Southwest Pacific Ocean. *Geographia Technica 14 (2)*, 39–48. https://doi.org/10.21163/GT_2019.142.04

Lemenkova, P. 2019e. Geomorphological modelling

and mapping of the Peru-Chile Trench by GMT. *Polish Cartographical Review 51 (4)*, 181–194. https://doi.org/10.2478/pcr-2019-0015

Lemenkova, P. 2019f. Automatic Data Processing for Visualising Yap and Palau Trenches by Generic Mapping Tools. *Cartographic Letters 27 (2)*, 72–89. https://doi.org/10.6084/m9.figshare.11544048

Lemenkova, P. 2020a. GEBCO and ETOPO1 gridded datasets for GMT based cartographic mapping of Hikurangi, Puysegur and Hjort Trenches, New Zealand. *Acta Universitatis Lodziensis. Folia Geographica Physica 19*, 7–18. https://doi.org/10.18778/1427-9711.19.01

Lemenkova, P. 2020b. Variations in the bathymetry and bottom morphology of the Izu-Bonin Trench modelled by GMT. *Bulletin of Geography. Physical Geography Series 18 (1)*, 41–60. https://doi.org/10.2478/bgeo-2020-0004

Lemenkova, P. 2020c. GEBCO Gridded Bathymetric Datasets for Mapping Japan Trench Geomorphology by Means of GMT Scripting Toolset. *Geodesy and Cartography 46 (3),* 98–112. https://doi.org/10.3846/gac.2020.11524

Lemenkova, P. 2021a. Geodynamic setting of Scotia Sea and its effects on geomorphology of South Sandwich Trench, Southern Ocean. *Polish Polar Research 42 (1)*, 1–23. https://doi.org/10.24425/ppr.2021.136510

Lemenkova, P. 2021b. Exploring structured scripting cartographic technique of GMT for ocean seafloor modelling: A case of the East Indian Ocean. *Maritime Technology and Research 3 (2)*, 162–184. https://doi.org/10.33175/mtr.2021.248158

Lemenkova, P. 2021c. Data-driven insights into correlation among geophysical setting, topography and seafloor sediments in the Ross Sea, Antarctic. *Caderno de Geografia 31 (64)*, 1–20. https://doi.org/0.5752/p.2318-2962.2021v31n64p1

Lemenkova, P., Promper, C., Glade, T. 2012. Economic Assessment of Landslide Risk for the Waidhofena.d. Ybbs Region, Alpine Foreland, Lower Austria. In: Eberhardt, E., Froese, C., Turner, A.K. & Leroueil, S. (eds.). *Protecting Society through Improved Understanding. 11th International Symposium on Landslides & the 2nd North American Symposium on Landslides & Engineered Slopes (NASL),* Banff, Canada, 279–285. https://doi.org/10.6084/m9.figshare.7434230

Lemoine, F.G., Kenyon, S.C., Factor, J.K., Trimmer, R.G., Pavlis, N.K., Chinn, D.S., Cox, C.M., Klosko, S.M., Luthcke, S.B., Torrence, M.H., Wang, Y.M., Williamson, R.G., Pavlis, E.C., Rapp, R.H., Olson, T.R. 1998. *NASA/TP-1998-206861: The Development of the Joint NASA GSFC and NIMA Geopotential Model EGM96*, NASA Goddard Space Flight Center, Greenbelt, Maryland, 20771 USA.

Liakopoulou-Morris, F., Main, I.G., Pearce, R.G. 1995. Source parameters of earthquakes in the Aleutian Islands subduction zone. *Geophysical Journal International 120 (2)*, 419–432. https://doi.org/10.1111/j.1365-246X.1995.tb01829.x

Litvin, V.M. 1987. *Morpho structure of the ocean seafloor*. Leningrad: Nedra.

López, A.M., Okal, E.A. 2006. A seismological reassessment of the source of the 1946 Aleutian 'tsunami' earthquake. *Geophysical Journal International 165 (3)*, 835–849. https://doi.org/10.1111/j.1365-246X.2006.02899.x

Lundgren, P., Saucier, F., Palmer, R., Langon, M. 1995. Alaska crustal deformation: Finite element modelling constrained by geologic and very long baseline interferometry data. *Journal of Geophysical Research 100 (B11)*, 22033–22045. https://doi.org/10.1029/95JB00237

Mortera Gutiérrez, C.A., Scholl, D.W., Carlson, R.L. 2003. Fault trends on the seaward slope of the Aleutian Trench: Implications for a laterally changing stress field tied to a westward increase in oblique convergence. *Journal of Geophysical Research 108 (B10)*, 2477. https://doi.org/10.1029/2001JB001433

Murray, H.W. 1945. Profiles of the Aleutian Trench. *Geological Society of America Bulletin 56 (7),* 757–782.

Müller, R.D., Seton, M., Zahirovic, S., Williams, S.E., Matthews, K.J., Wright, N.M., Shephard, G.E., Maloney, K.T., Barnett Moore, N., Hosseinpour, M., Bower, D.J., Cannon, J. 2016. Ocean basin evolution and global scale plate reorganization events since Pangea breakup. *Annual Review of Earth and Planetary Sciences 44 (1)*, 107–138. https://doi.org/10.1146/annurevearth060115012211

Müker, C., Wöner, G., Yogodzinski, G., Churikova, T. 2004. Behaviour of high field strength elements in subduction zones: constraints from Kamchatka-Aleutian arc lavas. *Earth and Planetary Science Letters 224*, 275–293. https://doi.org/10.1016/j.epsl.2004.05.030

Pullar, D., Egenhofer, M.J. 1988. Towards formal definitions of spatial relationships among spatial objects. *Proceedings of the 3rd International Symposium on Spatial Data Handling.* Sydney: IGU, 225–242.

Rathburn, A.E., Levin, L.A., Tryon, M., Gieskes, J.M., Martin, J.B., Pérez, M.E., Fodrie, F.J., Neira, C., Fryer, G.J., Mendoza, G., McMillan, P.A., Kluesner, J., Adamic, J., Ziebis, W. 2009. Geological and biological heterogeneity of the Aleutian margin (1965–4822 m). *Progress in Oceanography 80 (1–2)*, 22–50. https://doi.org/10.1016/j.pocean.2008.12.002

Rew, R.K., Davis, G.P. 1990. NetCDF: an interface for scientific data access. *IEEE Computer Graphics and Applications 10 (4)*, 76–82. https://doi.org/10.1109/38.56302

Ryan, H.F., von Huene, R., Wells, R.E., Scholl, D.W., Kirby, S., Draut, A.E. 2012. *History of earthquakes and tsunamis along the eastern Aleutian-Alaska mega thrust, with implications for tsunami hazards in the California Continental Borderland*. In: Dumoulin, J.A., Dusel-Bacon, C. (eds.), *Studies by the U.S. Geological Survey in Alaska*, *2011*, *USGS Professional Paper 1795–A*. https://pubs.usgs.gov/pp/1795/a/

Sandwell, D.T., Smith, W.H.F. 1997. Marine gravity anomaly from Geosat and ERS 1 satellite altimetry. *Jour-*

nal of Geophysical Research 102 (B5), 10039–10054. https://doi.org/10.1029/96JB03223

Seton, M., Flament, N., Whittaker, J., Müller, R.D., Gurnis, M., Bower, D.J. 2015. Ridge subduction sparked reorganization of the Pacific plate mantle system 60–50 million years-ago. *Geophysical Research Letters 42*, 1732–1740. https://doi.org/10.1002/2015GL063057

Schenke, H.W., Lemenkova, P. 2008. Zur Frage der Meeresboden-Kartographie: Die Nutzung von AutoTrace Digitizer für die Vektorisierung der Bathymetrischen Daten in der Petschora-See. *Hydrographische Nachrichten 81*, 16–21. https://doi.org/10.6084/m9.figshare.7435538

Schmid, F., Kopp, H., Schnabel, M., Dannowski, A., Heyde, I., Riedel, M., Hannington, M.D., Engels, M., Beniest, A., Klaucke, I., Augustin, N., Brandl, P.A., Devey, C. 2020. Crustal structure of the Niuafo'ou Microplate and Fonualei Rift and Spreading Center in the northeastern Lau Basin, Southwestern Pacific. *Journal of Geophysical Research: Solid Earth 125*, e2019JB019184. https://doi.org/10.1029/2019JB019184

Shepard, F.P. 1963. *Submarine Geology*. New York: Harper & Row.

Smith, W.H.F. 1993. On the accuracy of digital bathymetric data. *Journal of Geophysical Research 98 (B6)*, 9591–9603. https://doi.org/10.1029/93JB00716

Smith, W.H.F., Sandwell, D.T. 1997. Global Sea Floor Topography from Satellite Altimetry and Ship Depth Soundings. *Science 26*, *277 (5334),* 1956–1962 https://doi.org/10.1126/science.277.5334.1956

Suetova, I.A., Ushakova, L.A., Lemenkova, P. 2005. Geoinformation mapping of the Barents and Pechora Seas. *Geography and Natural Resources 4*, 138–142. https://doi.org/10.6084/m9.figshare.7435535

Tibaldi, A., Bonali, F.L. 2017. Intra-arc and back-arc volcano-tectonics: Magma pathways at Holocene Alaska-Aleutian volcanoes. *Earth-Science Reviews 167*, 1–26. https://doi.org/10.1016/j.earscirev.2017.02.004

Torne, M., Jiménez-Munt, I., Vergés, J., Fernàndez, M., Carballo, A., Jadamec, M. 2020. Regional crustal and lithospheric thickness model for Alaska, the Chukchi shelf, and the inner and outer Bering shelves. *Geophysical Journal International 220 (1)*, 522–540. https://doi.org/10.1093/gji/ggz424

Udintsev, G.B. 1972. Geomorfologija I tektonika dnaTihogo okeana [Geomorphology and seafloor tectonics of the Pacific Ocean]. Moscow, Nauka, 394 p. [In Russian].

Udintsev G.B. 1987. Rel'yef I stroyeniye dna okeanov [The relief and structure of the ocean floor]. Moscow, Nedra, 239 pp. [In Russian].

Udintsev, G.B., Boychenko, I.G., Kanaev, V.F. 1959. Rel'ef dna Beringova morja [Seafloor relief of the Bering Sea]. *Proceedings of IO AN USSR 29*, 17–64. [In Russian].

Udintsev, G.B., Agapova, G.V., Beresnev, A.F. 1963. Novaja batimetricheskaja karta Tihogo okeana [New bathymetric map of the Pacific Ocean]. *II Oceanological research 9*, 60–101. [In Russian].

Udintsev, G.B., Beresnev, A.F., Gordin, V.M. 1980. Strukturnaya neodnorodnost' dna Mirovogo okeana I problema granitsy okean-materik [Structural heterogeneity of the bottom of the oceans and the problem of the ocean-continent boundary]. *Geotectonics 2*, 13–26. [In Russian].

Vaes, B., van Hinsbergen, D.J.J., Boschman, L.M. 2019. Reconstruction of subduction and backarc spreading in the NW Pacific and Aleutian Basin: Clues to causes of Cretaceous and Eocene plate reorganizations. *Tectonics 38*, 1367–1413. https://doi.org/10.1029/2018TC005164

Vasquez, M., Chacón, D.M., Tempera, F., O'Keeffe, E., Galparsoro, I., Sanz Alonso, J.L., Gonçalves, J.M.S., Bentes, L., Amorim, P., Henriques, V., McGrath, F., Monteiro, P., Mendes, B., Freitas, R., Martins, R., Populus, J. 2015. Broad-scale mapping of seafloor habitats in the north-east Atlantic using existing environmental data. *Journal of Sea Research 100*, 120–132. https://doi.org/10.1016/j.seares.2014.09.011

Wadge, G. 1992. GIS for geology. *Terra Nova 3 (1)*, 93–98.

Watts, A.B., Talwani, M. 1974. Gravity Anomalies Seaward of Deep-Sea Trenches and their Tectonic Implications. *Geophysical Journal International 36 (1)*, 57–90. https://doi.org/10.1111/j.1365-246X.1974.tb03626.x

Wessel, P., Watts, A.B. 1988. On the accuracy of marine gravity measurements. *Journal of Geophysical Research 93*, 393–413. https://doi.org/10.1029/JB093iB01p00393

Wessel, P., Smith, W.H.F. 1991. Free software helps map and display data. *Eos Transactions of the American Geophysical Union 72 (41)*, 441–446. https://doi.org/10.1029/90EO00319

Wessel, P., Smith, W.H.F. 1995. New version of the Generic Mapping Tools released. *Eos Transactions of the American Geophysical Union 76 (33)*, 329. https://doi.org/10.1029/95EO00198

Wessel, P., Smith, W.H.F. 1996. A Global Self-consistent, Hierarchical, High-resolution Shoreline Database. *Journal of Geophysical Research 101*, 8741–8743. https://doi.org/10.1029/96JB00104

Wessel, P., Smith, W.H.F., Scharroo, R., Luis, J.F., Wobbe, F. 2013. Generic mapping tools: Improved version released. *Eos Transactions AGU 94 (45)*, 409–410. https://doi.org/10.1002/2013EO450001

Yogodzinski, G.M., Brown, S.T., Kelemen, P.B., Vervoort, J.D., Portnyagin, M., Sims, K.W.W., Hoernle, K., Jicha, B.R., Werner R. 2015. The role of subducted Basalt in the Source of Island Arc Magmas: evidence from seafloor Lavas of the Western Aleutians. *Journal of Petrology 56*, 441–492. https://doi.org/10.1093/petrology/egv006

Yoshida, M. 2017. Trench dynamics: Effects of dynamically migrating trench on subducting slab morphology and characteristics of subduction zones systems. *Physics of the Earth and Planetary Interiors 268*, 35–53. https://doi.org/10.1016/j.pepi.2017.05.004